Supporting Information

Synthesis and Self-assembly of Amphiphilic Precision Glycomacromolecules

*Alexander Banger, Julian Sindram, Marius Otten, Jessica Kania, Dimitri Wilms, Alexander Strzelczyk, Sean Miletic, Thomas Marlovits, Matthias Karg and Laura Hartmann**

Materials:

All chemicals were commercially available. The resins Fmoc-AA-TentaGel® S TRT loading 0.21 mmol/g and Tentagel® S RAM loading 0.24 mmol/g were bought from RAPP Polymers and. Trifluoroacetic acid 99%, diethylenetriamine 99%, hexamethylendiamine 98%, ethyltrifluoroacetate 99%, triisopropylsilane 99%, maleic acid 99%, sodium L-ascorbate, 2,2-dimethoxy-2-phenylacetophenone (DMPA) 99%, α-D-mannose 99%, deuterated Methanol (MeOD), dimethylsulfoxide (DMSO-d_6), deuterated water (D_2O) and chloroform ($CDCl_3$) were bought from Sigma-Aldrich. 9-Fluorenylmethyl chloroformate, piperidine 99%, Lauric acid 99%, DIPEA 98%, Divinylbenzene for synthesis, Sodium Hydroxide for analysis were bought from Merck. Copper(II) sulfate 98% pure anhydrous, Piperidine 99% from Acros. Rhodamine

labeled ConA was bought from vector laboratories. D-(+)-galactose (pure) were purchased from AppliChem. PyBOP (Benzotriazol-1-yloxy)tripyrrolidinophosphonium hexafluorophosphate >98% was bought from Carbosynth. Decanoic acid 99% was bought from J&K. Pentadecanoic acid was bought from Alfa Aesar. The chemicals were, if not mentioned otherwise used without further purification. HPLC grade solvents were used throughout all reactions.

Instrumentation

Nuclear magnetic resonance spectroscopy

^{1}H-NMR and ^{13}C-NMR measurements were performed using a Bruker Avance III 300 and Bruker Avance III 600 spectrometer operating at 300 MHz and 600 MHz for the ^{1}H NMR and at 75 MHz and 150 MHz for the ^{13}C-NMR at room temperature if not otherwise noted. The signals of the incompletetly deuterated solvents were used as internal standard. The spin multiplicities were abbreviated with s (singlet), d (doublet), t (triplet) and m (multiplet). The chemical shifts (δ) were stated in parts per million (ppm) and coupling constants (*J*) were stated in hertz (Hz). For data analysis MestReNova 10.0.2 was used.

Mass spectroscopy

HR-MS (ESI) spectra were recorded on an Ion-Trap-API Finningan LCQ Deca (Thermo Quest) mass spectrometer. Ionization was carried out by electrospray ionization. All samples were measured in concentration of 1 mg/ml.

Reversed Phase High Pressure Liquid Chromatography coupled with ESI Mass Spectrometry

RP-HPLC-MS was carried out on an Agilent 1260 Infinity instrument coupled to a variable wavelength detector (VWD) and a 6120 Quadrupole LC/MS containing an Electrospray Ionization (ESI) source (operation mode positive and negative, m/z range from 200 to 2000). A MZ-AquaPerfect C18 (3.0 × 50 mm, 3 µm) RP column from Mz-Analysentechnik GmbH was used with a flow rate of 0.4 ml/min at 25 °C. As eluent system water/acetonitrile containing 0.1% formic acid was applied.

Thin layer chromatography

Thin layer chromatography (TLC) was performed on silicia gel coated aluminium sheets from Merk (60 F_{254} 0.25mm). The detection was carried out via UV irradtion and with a ninhydrin staining followed by heating or an iodine chamber.

Freeze drying

Samples were dissolved in water, frozen with liquid nitrogen and then freeze dried with an Alpha 1-4 LD plus instrument from Martin Christ Freeze Dryers GmbH.

Fluorescence spectroscopy

The fluorescence measurements were conducted using the FLS980 Fluorometer from Edinburgh Instruments and with a CLARIOstar plate reader from BMG Labtech.

Fluorescence microscopy

An inverted microscope (Olympus IX73, Japan) equipped with an Olympus 60× NA 1.35 oil-immersion objective (Olympus, Japan), and a CMOS camera (DMK 33UX174L, the Imaging Source, Germany) was used for the fluorescence microscopy.

Light scattering

For the light scattering measurements, a 3D LS Spectrometer from LS Instruments (Fribourg, Switzerland) was used in 2D pseudo cross-correlation operation. The instrument is equipped with a HeNe laser as light source (max. output power of 35 mW at λ = 632.8 nm). A quartz vet filled with decalin serves as temperature and refractive index matching bath. The setup is equipped with two Glan-Thompson prisms (extinction ratio of 10^{-6}), one in front of the sample and one in front of the detector. For depolarized dynamic light scattering (DDLS) measurements, the prism in front of the detector was turned by 90° and finely adjusted until minimal scattering intensity was detected using an isotropic scatterer. Analysis of the data were carried out using the cumulant method after Frisken.

Atomic force microscopy

For the AFM measurements a NanoWizard II from JPK instruments was used. The data was analyzed using JPKSPM analysis Software.

Electron Microscopy

Transmission electron microscopy was performed on a JEOL JEM-2100Plus operating in bright-field mode at 80 kV acceleration voltage. Images were analyzed using GMS 3.

UV-lamp

A TQ150 Hg medium pressure UV lamp from Heraeus Nobellight GmbH with a quartz glass immersion and cooling tube from Peschl Ultraviolet GmbH was used for micelle crosslinking

General Methods

Solid phase synthesis

For the solid phase assembly, a Fmoc Gly TentaGel® R Trt resin (prefunctionalised) with a loading of 0.21 mmol/g and a TentaGel® S RAM resin with a loading of 0.22 mmol/g was used as a solid support for the synthesis. The reactions were carried out on a scale between 0.05 and 0.20 mmol. As reaction vessels, polypropylene syringes with a porous polypropylene frit at the bottom were used. Before the first reaction step the resin was swollen two times for 15 minutes with DCM and then the solvent was changed to dimethylformamide (DMF) by washing the resin multiple times with DMF.

Solid phase building block and sugar synthesis

Solids phase building blocks as well as sugar azides were synthesized according to literature.[1, 2] However, during sugar synthesis additional precaution is required as with 2-bromoethanol and 2-chloroethanol, two highly toxic substances are used.

General Coupling protocol

The deprotection of the primary amine was performed with a solution of 25% piperidine in DMF two times, once for 5 and once for 15 minutes. Therefore at least 5 ml of the solution were added to the reaction vessel. Afterwards, the resin was washed at least 10 times with DMF. Then the coupling was performed by dissolving 5 equivalents of the used building block and 4.9 of PyBOP in 1 to 2 ml DMF (depending on the batch size) and 20 equivalents of DIPEA were added. The whole solution was vortexed to ensure complete dissolution. Afterwards, the solution was added to the reaction vessel and shaken for 1 hour. Then the mixture was washed

five times with DMF and the coupling protocol is repeated, or the compound is cleaved of the solid support.

CuAAC protocol for solid phase copper mediated azide-alkyne cycloaddition

The CuAAC reaction was performed with 3 equivalents of the alkyne sugar regarding the azide groups on the backbone. Furthermore, 12 mg of copper sulfate and 12 mg of sodium ascorbate were used for all sugars except for sialic acid. For sialic acid the amount was increased to 50 mg of each compound because of its complexing properties. The sugar was solved in DMF and the other two compounds in water, so that the final ratio was 2 equivalents DMF and 1 equivalents water. Then all solutions were added to the reactions vessel and shaken for 24 h. Afterwards, the resin was washed with water and DMF several times. Also, the resin was washed with a solution of dithiocarbamate order to remove the remaining copper ions.

Sugar deprotection and cleavage from solid support

For the glycine loaded resin the sugar moiety was deprotected and at the same time the oligomer was cleaved off the resin using 0.05 M NaOH.

For the S RAM resin the sugar was deprotected using 0.05 M NaOMe two times for 20 minutes. Cleavage was achieved with a solution of 95% TFA, 2.5% DCM and 2.5 % TIPS (*v/v*). The cleavage solution was precipated in ether, centrifuged, dried and dialysed against MQ Water (100-500 MWCO).

Core-crosslinking of the micelles

A stock solution of DVB (1 mg/ml) and DMPA (12.8 mg/ml) in DCM was prepared. Then 100 µL of the DVB and 10 µL DMPA stock solution was added to a falcon tube. The DCM was allowed to evaporate over a Nitrogen-flow. Following a solution of 4 mg oligomer dissolved in 0.8 ml ultrapure water (approximately 5 mM) was added to the falcon tube. The reaction mixture was shaken until all compounds were dissolved. Subsequently, the solution was degassed with argon for at least 20 minutes, transferred to a quartz reactor, sealed with Parafilm and immediately irradiated with a mercury lamp. Afterwards, the solution was purified in a dialysis tube MWCO 3.5 kDa in deionized water/ethanol 1:1 (*v/v*) (three solvent switches) followed by three solvent switches with deionized water.

AFM imaging

AFM experiments were conducted for the non-crosslinked micelles and for the crosslinked micelles. For the AFM experiments glass, silicon and mica surfaces were used. Prior to their usage glass and silicon surfaces were cleaned following a RCA-cleaning protocol. Samples were applied via drop or spin coating. AFM imaging was performed in air and the NanoWizard II was used in tapping mode. Commercial silicon probes were used with a nominal force constant of 7 n/m at a resonance frequency of about 155 kHz.

TEM imaging

7 microliters of the respective aqueous sample dispersion were applied to continuous carbon grids for 1 minute. After blotting, grids were placed on a drop of 3% uranyl acetate solution

and immediately blotted. Then the grid was placed again on a drop of 3% uranyl acetate solution, this time for 30 seconds. After blotting the grid was dried for 20 minutes.

Fluorescence binding study

A rhodamine labeled ConA stock solution of 1mg/ml was prepared in lectin binding buffer (10 mM Hepes, 50 mM NaCl, 1 mM $MnCl_2$, 1 mM $CaCl_2$, pH 7.4). 1 µL of this solution was added to a solution of 5 mM APG 8 also in LBB. This mixture was incubated for 30 minutes and afterwards directly measured with a fluorescence Microscope.

Bacteria adhesion assay

The assay was adapted from literature. [3] In short black 96-well plates were coated with mannan solution (1.5 mg/ml) in carbonate buffer and dried in an incubator at 37°C overnight. The plate was washed three times with PBST (PBS + 0.05 % Tween 20) and blocked with 5% BSA in PBS for 2 hours. The plate is washed again three time with PBST and once with PBS. This was followed by adding the oligomer solutions and then the bacteria (*E. coli* PKL1162)s (2 mg/ml). The plate was incubated for 4.5 hours at 37°C with a closed lid. Plates were washed three times with PBS and then filled up with PBS 100µl/well. Finally, fluorescence intensity was measured with a Clariostar plate reader at 485 nm excitation and 535 nm emission.

Analytical Data:

1. Synthesis of HDM:

The newly developed building block HDM was synthesized in a four-step procedure similar to the synthesis of EDS[2]. The overall yield of the synthesis was 10%.

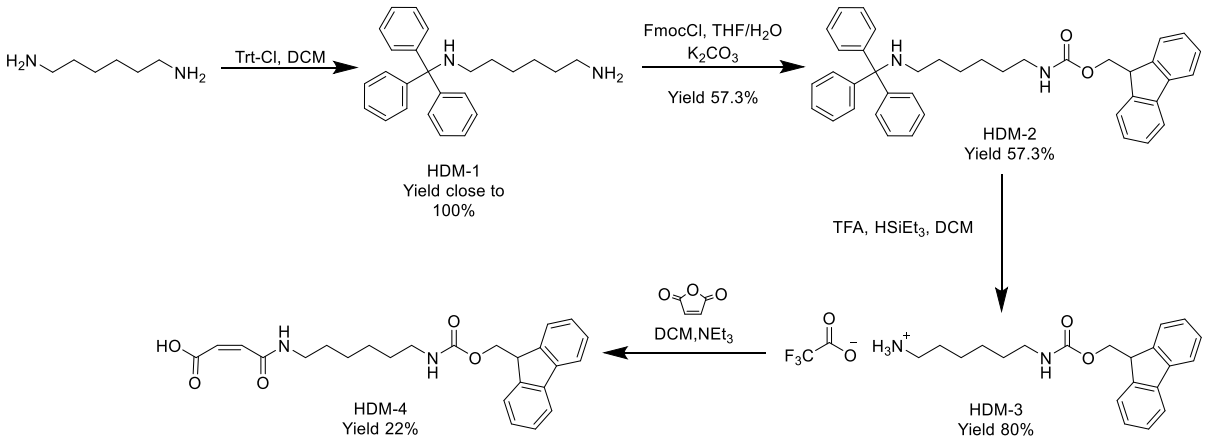

Figure S1. Overview of the synthesis of the HDM building block.

N[1]-tritylhexane-1,6-diamine, **HDM-1**

50 g (430 mmol) hexamethylenediamine was dissolved in 400 ml DCM. Then 24 g (86 mmol) tritylchloride was dissolved in 200 ml DCM and added drop wise over a period of 2 h to the ice-cooled solution of hexamethylenediamine while being stirred. After the addition, the mixture was allowed to reach RT and stirred for additional 2 h. The organic solution was concentrated to 200 ml in vacuo and washed three times with 100 ml sat. aqueous sodium bicarbonate solution. Then the solution was dried over $MgSO_4$, filtered and concentrated in vacuo and dried in high vacuo to give a yellowish oil. The product was used in the next step without further purifications.

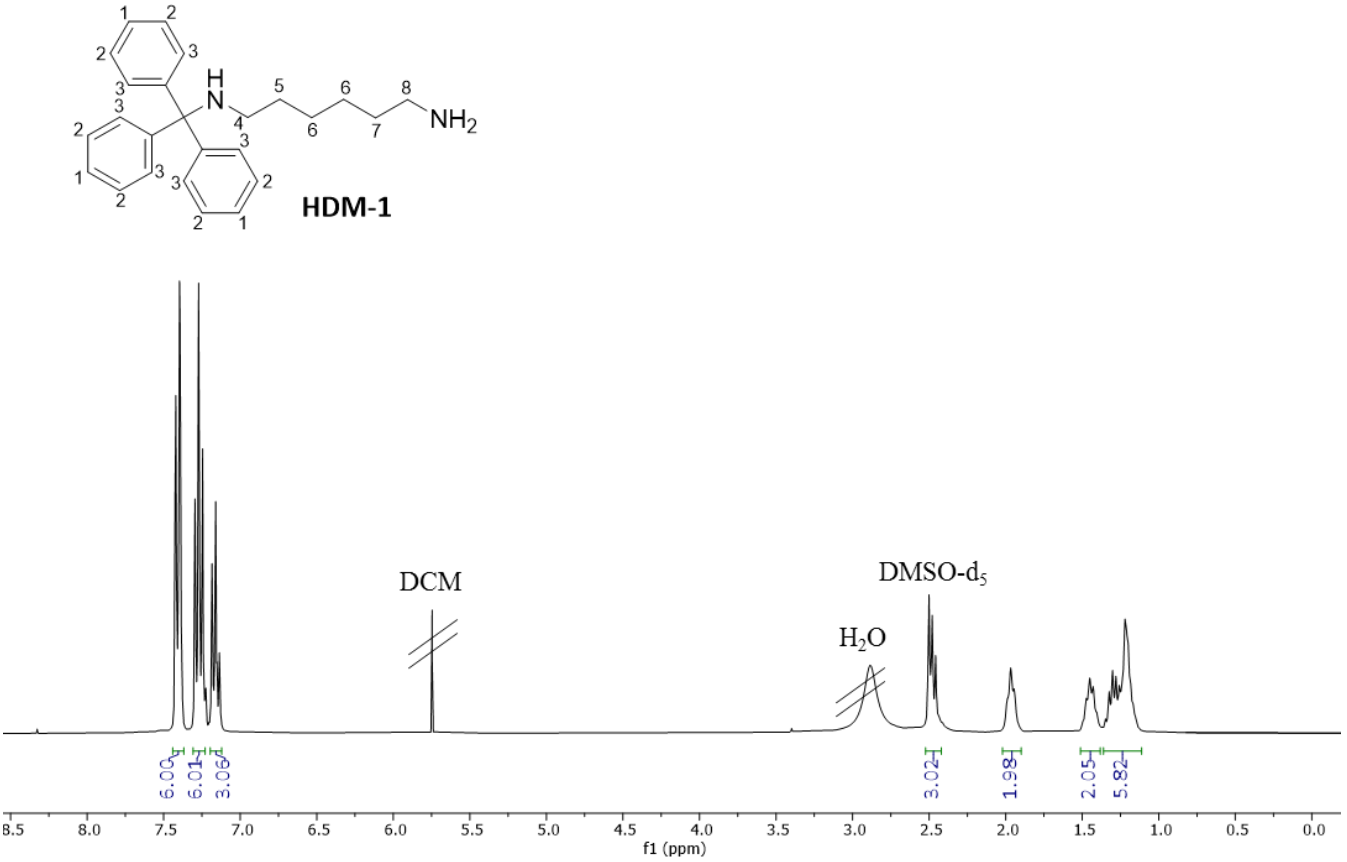

Figure S2. [1]H-NMR spectrum of HDM-1 recorded in DMSO-d6. The individual protons are assigned by number.

[1]H NMR (300 MHz, DMSO-d_6): δ (ppm) 7.45 – 7.36 (m, 6H, 2), 7.32 – 7.21 (m, 6H, 3), 7.20 – 7.11 (m, 3H, 1), 2.54 – 2.41 (m, 2H, overlap with DMSO signal, 8), 2.01 – 1.91 (m, 2H, 4), 1.52 – 1.38 (m, 2H, 7), 1.36 – 1.12 (m, 6H, 5, 6).

ESI-MS for HDM 1 (Monoisotopic mass: 358.2 g/mol): Found 359.3 g/mol, $M+H]^+$.

(9H-fluoren-9-yl)methyl (6-(tritylamino)hexyl)carbamate, **HDM-2**

All of HDM-1 was dissolved in one portion in a mixture of 29.7 g (215 mmol) K_2CO_3 and 100 ml deionized water. Then 300 ml of THF were added (ratio of H_2O to THF = 1:3, *v/v*) and after that FmocCl was added in one portion under rigorous stirring. The reaction progress was monitored by TLC (EtOAc:nHex = 1:1, *v/v*). After complete conversion, 100 ml of EtOAc were added to the mixture. Finally, the aqueous phase was extracted twice with EtOAc (2 x 100 ml). Afterwards the organic phase was washed with brine, dried over $MgSO_4$ and concentrated in vacuo. The gel type product was recrystallized from Et_2O. 22.3 g (49.29 mmol, 57.3 %) of the pure product were obtained as a fine white powder.

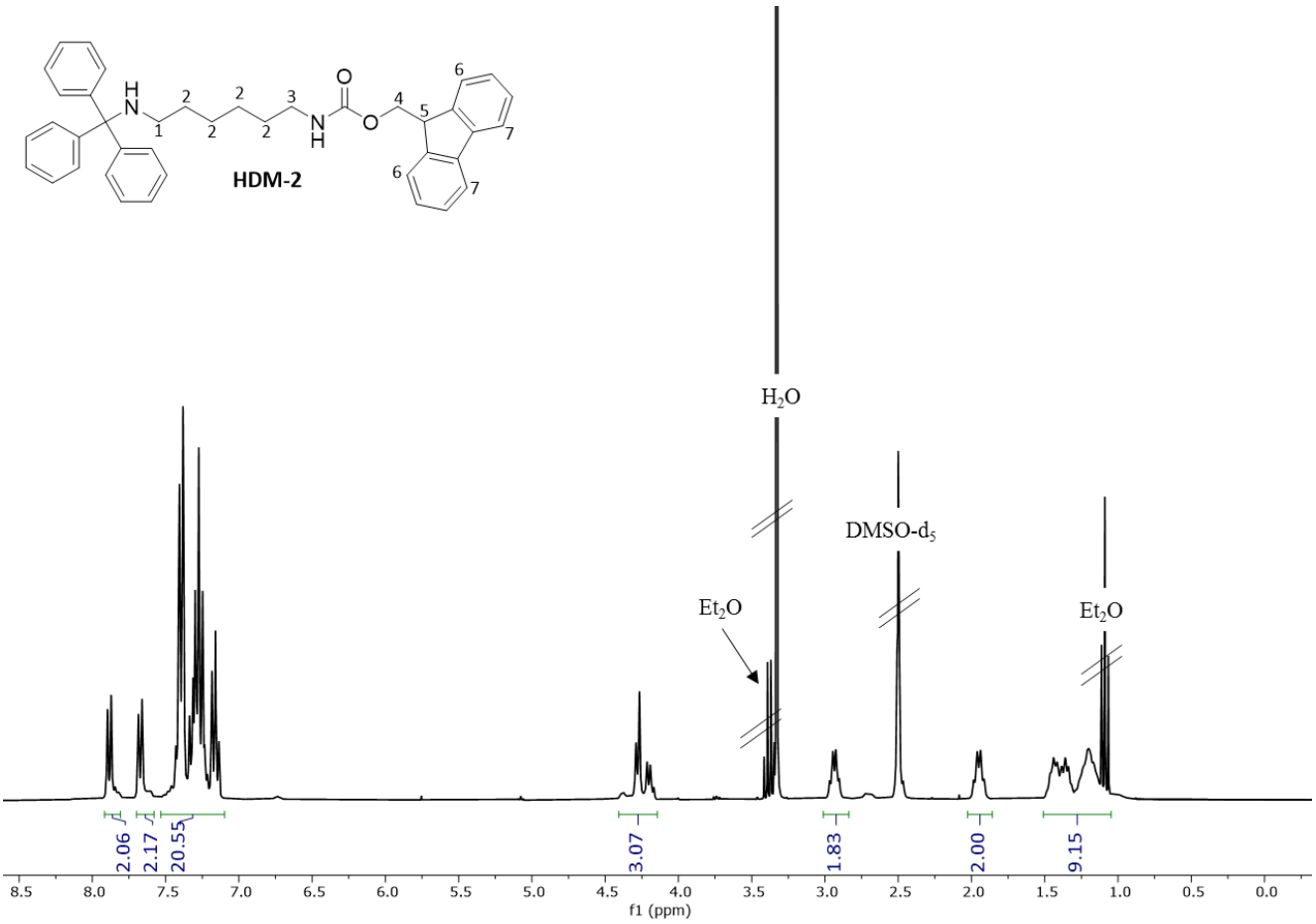

Figure S3. ^{1}H-NMR spectrum of HDM-2 recorded in DMSO-d6. The individual protons are assigned by number.

^{1}H NMR (300 MHz, DMSO-d_6): δ (ppm) 7.88 (d, *J* = 7.4 Hz, 2H, 7), 7.67 (d, *J* = 7.4 Hz, 2H, 6), 7.51 – 7.11 (m, 20H, rest of the aromatic protons), 4.41 – 4.16 (m, 3H, 4, 5), 3.04 – 2.85 (m, 2H, 3), 2.03 – 1.86 (m, 2H, 1), 1.53 – 1.06 (m, 8H (overlap with Et_2O rest)).

ESI-MS for HDM 2 (Monoisotopic mass: 580.3 g/mol): Found 581.3 g/mol, $[M+H]^+$.

RP-HPLC (linear gradient from 5-95% acetonitrile in water in 30 min at 25°C): t_R = 10.48 min.

Determined relative purity: 96.1%

6-((((9H-fluoren-9-yl)methoxy)carbonyl)amino)hexan-1-ammonium 2,2,2-trifluoroacetate,

HDM-3

22.3 g (49.29 mmol) of HDM-2 were dissolved in a mixture of 100 ml DCM and 10 ml triethylsilane, before 20 ml trifluoroacetic acid was added carefully while stirring at moderate speed. The reaction is exothermal and was cooled to room temperature. The reaction turned yellow to orange while adding TFA and turned clear again after complete conversion. The reaction progress was controlled with TLC (EtOAc:*n*-Hexan = 1:1, *v/v*) using ninhydrin staining to confirm complete conversion. The mixture was precipitated into 200 ml diethyl ether and a gel type product was formed. After complete precipitation of the product (usually in the fridge overnight) all solvents were decanted off and the residue was dried in vacuo. 18 g (40 mmol) were isolated, which corresponded to a yield of 80 %.

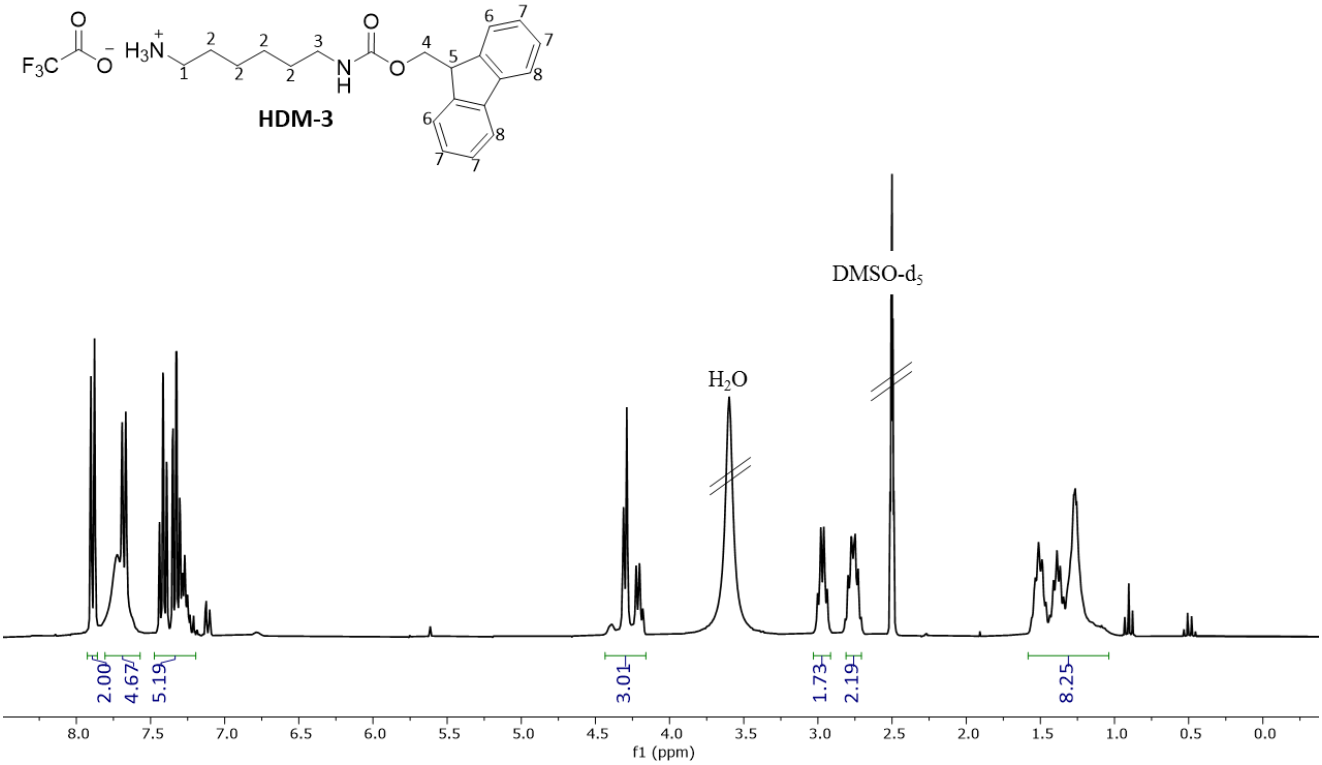

Figure S4. ^{1}H-NMR spectrum of HDM-3 recorded in DMSO-d6. The individual protons are assigned by number.

^{1}H NMR (300 MHz, DMSO-d$_6$): δ (ppm) 7.89 (d, J = 7.3 Hz, 2H, 8), 7.82 – 7.61 (m, 2H, 6(overlap with the amine signal)), 7.46 – 7.21 (m, 5H, 7), 4.43 – 4.16 (m, 3H, 4, 5), 3.04 – 2.91 (m, 2H, 1), 2.85 – 2.67 (m, 2H, 3), 1.60 – 1.04 (m, 8H, 2).

ESI-MS for HDM 3 (Monoisotopic mass: 339.2 g/mol): Found 340.3 g/mol, $[M+H]^+$.

RP-HPLC (linear gradient from 5-95% acetonitrile in water in 30 min at 25°C): t_R = 1.25 min.

Determined relative purity: 94%

(Z)-4-((6-((((9H-fluoren-9-yl)methoxy)carbonyl)amino)hexyl)amino)-4-oxobut-2-enoic acid, **HDM-4**

10 g (22.1 mmol) of HDM-3 was dissolved in 80 ml DCM and 5 ml of triethylamine was added. The solution was stirred for two hours. In the meantime, a solution of maleic anhydride was prepared by dissolving 1.9 g in 100 ml of DCM. After two hours the solution of HDM-3 was slowly added via a dropping funnel to the maleic anhydride solution over a period of four hours. Note that the mixture of will not dissolve completely, but by adding it to the maleic anhydride solution it will dissolve. Additionally, the usage of the dropping funnel is essential as maleic anhydride is prone to polymerization (solution will turn red upon polymerization). Finally, all solvents were removed in vacuo, the resulting foam was dissolved in 200 ml of EtOAc and as much 0.2 g/ml citric acid solution was added until PH 3-4 was reached. The aqueous layer was than extracted three times (3x 100 ml) with EtOAc, the combined organic phases were dried over $MgSO_4$ and concentrated in vacuo. The raw product was recrystallized from EtOAc and 2.08 g (4.8 mmol, 22 %) of the pure product was obtained as a fine white powder.

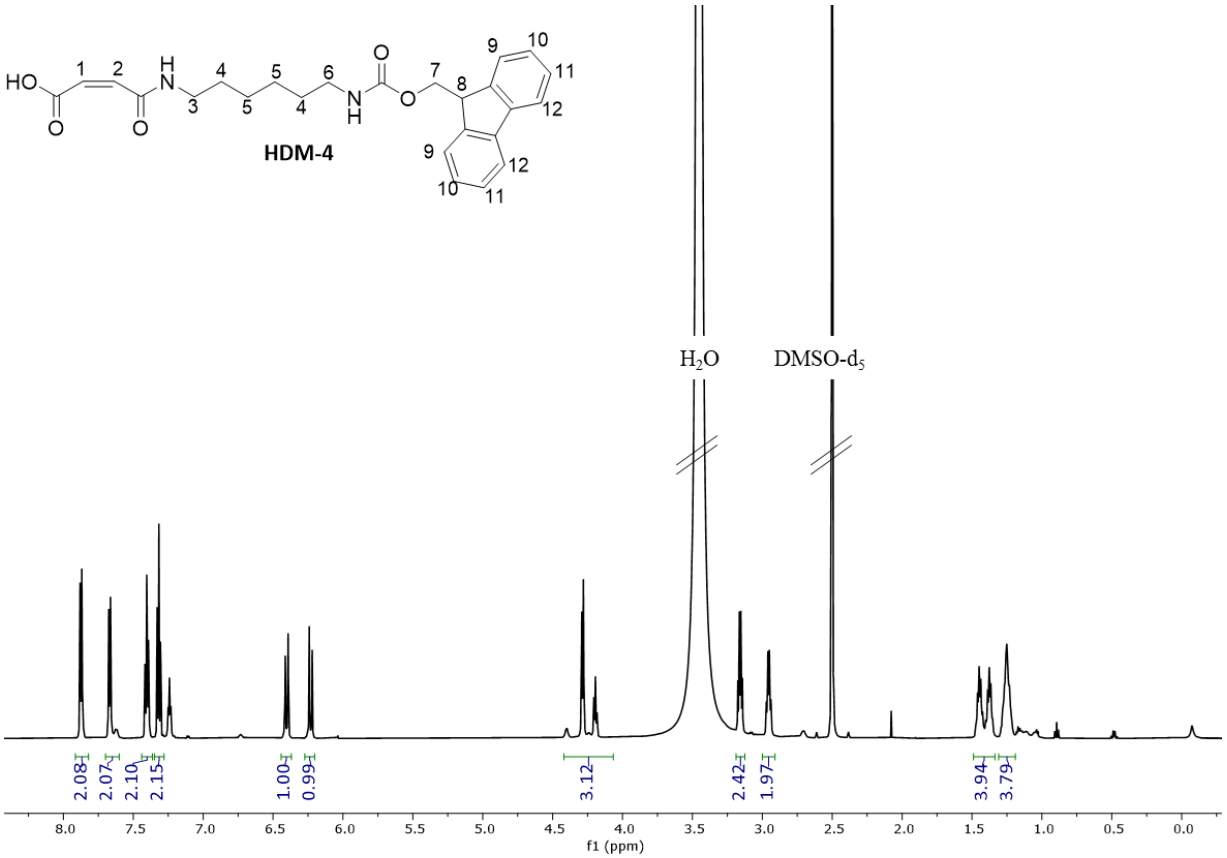

Figure S5. [1]H-NMR spectrum of HDM-4 recorded in DMSO-d6. The individual protons are assigned by number.

[1]H NMR (600 MHz, DMSO-d6): δ (ppm) 7.87 (d, J = 7.5 Hz, 2H, 12), 7.67 (d, J = 7.5 Hz, 2H, 9), 7.40 (t, J = 7.4 Hz, 2H, 11), 7.34 – 7.29 (m, 2H, 10), 6.40 (d, J = 12.6 Hz, 1H, 1), 6.23 (d, J = 12.5 Hz, 1H, 1), 4.32 – 4.16 (m, 3H, 7, 8), 3.16 (q, J = 6.7 Hz, 2H, 3 (overlap with residual solvent signal)), 2.96 (q, J = 6.6 Hz, 2H, 6), 1.49 – 1.34 (m, 4H, 4), 1.29 – 1.20 (m, 4H, 5).

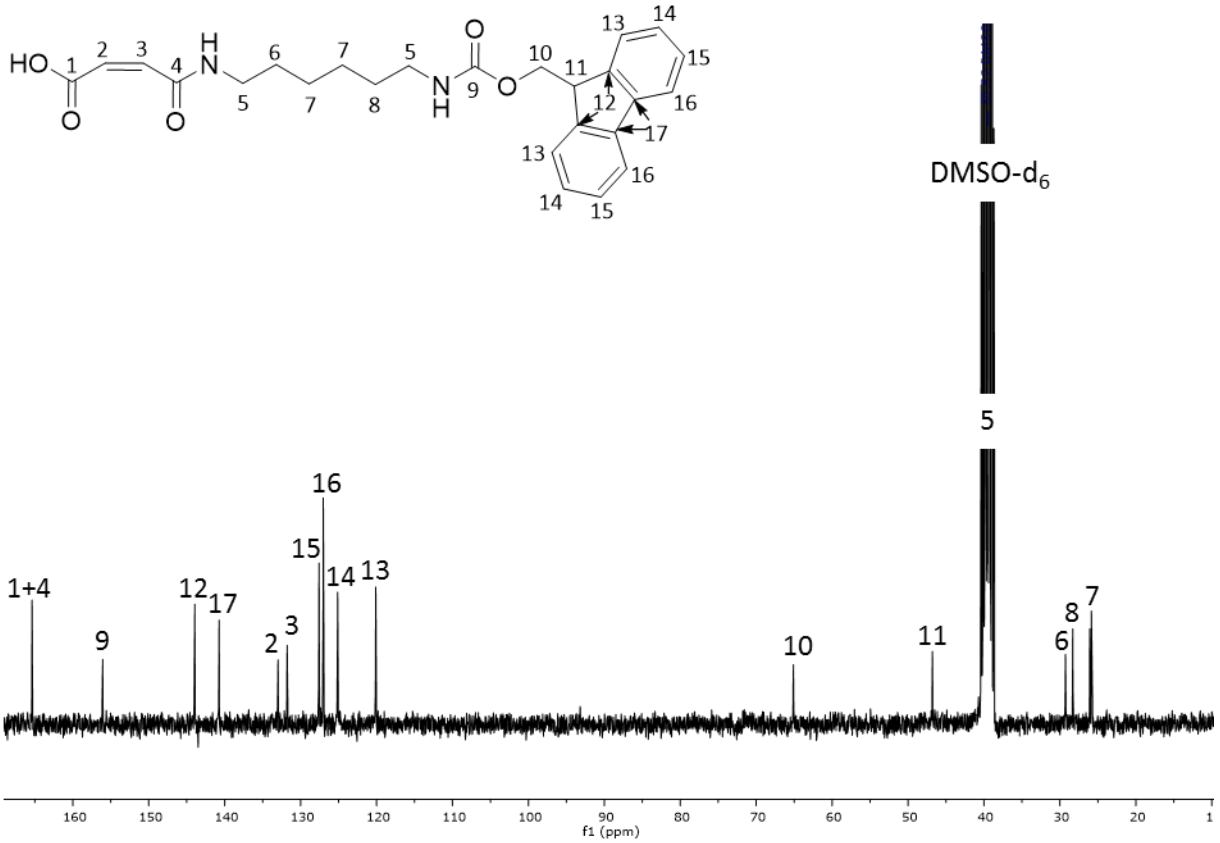

Figure S6 ^{13}C-NMR spectrum of HDM-4 recorded in DMSO-d6. The individual carbons are assigned by number.

^{13}C-NMR (75 MHz, DMSO): δ (ppm) 165.28 (C-1, C-4), 156.03 (C-9), 143.90 (C-12), 140.70 (C-17), 132.94 (C-2), 131.73 (C-3), 127.54 (C-15), 126.98 (C-16), 125.08 (C-14), 120.07 (C-13), 65.07 (C-10), 46.75 (C-11), 29.23 (C-6), 28.27 (C-8), 25.81 (C-7).

ESI-MS for HDM 4 (Monoisotopic mass: 436.2 g/mol): Found 437.2 g/mol, $[M+H]^+$.

RP-HPLC (linear gradient from 5-95% acetonitrile in water in 30 min at 25°C): t_R = 19.89 min.

Determined relative purity: 97%

Elementary analyses:

Table S1. Result of the elementary analyses of the new building block HDM

	Theoretical value	Analytical result
%C	68.79	68.40
%N	6.42	6.33
%H	6.47	6.47

4-((6-((((9H-fluoren-9-yl)methoxy)carbonyl)amino)hexyl)amino)-4-oxobutanoic acid **HDS-4**

10 g (22.1 mmol) of HDM-3 was dissolved in 200 ml DCM and 5 ml of triethylamine was added. Following 2.4 g (24.3 mmol) succinic anhydride was added at once and the solution was stirred overnight. Finally, all solvents were removed in vacuo, the resulting foam was dissolved in 200 ml of EtOAc and as much 0.2 g/ml citric acid solution was added until PH 3-4 was reached. The aqueous layer was than extracted three times (3x 100 ml) with EtOAc, the combined organic phases were dried over $MgSO_4$ and concentrated in vacuo. The raw product was recrystallized from EtOAc and 2.08 g (4.8 mmol, 22 %) of the pure product was obtained as a fine white powder.

^{1}H NMR (600 MHz, DMSO): δ (ppm) 7.87 (d, *J* = 7.5 Hz, 2H), 7.67 (d, *J* = 7.5 Hz, 2H), 7.40 (t, *J* = 7.4 Hz, 2H), 7.32 (t, *J* = 7.4, 2H), 4.28 (d, *J* = 6.9 Hz, 2H), 4.19 (t, *J* = 6.9 Hz, 1H), 2.99 (t, *J* = 7.0 Hz, 2H), 2.94 (t, *J* = 7.0 Hz, 2H), 2.41 (t, *J* = 7.0 Hz, 2H), 2.28 (t, *J* = 7.0 Hz, 2H), 1.39 – 1.19 (m, 8H).

ESI-MS for HDS 4 (Monoisotopic mass: 438.2 g/mol): Found 439.2 g/mol, $[M+H]^+$.

RP-HPLC (linear gradient from 5-95% acetonitrile in water in 30 min at 25°C): t_R = 17.5 min.

Determined relative purity: 99%

2. Oligomers

Table S2. Overview of the yields and relative purities of the synthesized APGs

APG	Average Yield	Relative Purity[2]
1	29%	>90%
2	22%	>90%
3	35%	>90%
4	32%	>90%
5	65%	>90%
6	30%	>95%
7	45%	>90%
8	34%	>95%[1]

[1]purified using preparative HPLC, [2]as determined by integration

APG **2**, Gly-TDS(Man)-HDM-C10

The integral for the multiplet between 3.9 – 2.9 is larger than expected, due to a baseline increase which is derived through the self-assembly nature of the material and an overlap with the solvent. In order to suppress the baseline increase as much as possible a solvent mixture of D_2O and CD_3OD was used. Furthermore, the integral for the alkene moiety of the HDM building block is decreased. Potentially this is due to the acidic nature of the alkene protons and that the protons are exchanged with deuterium, thus decreasing the integral.

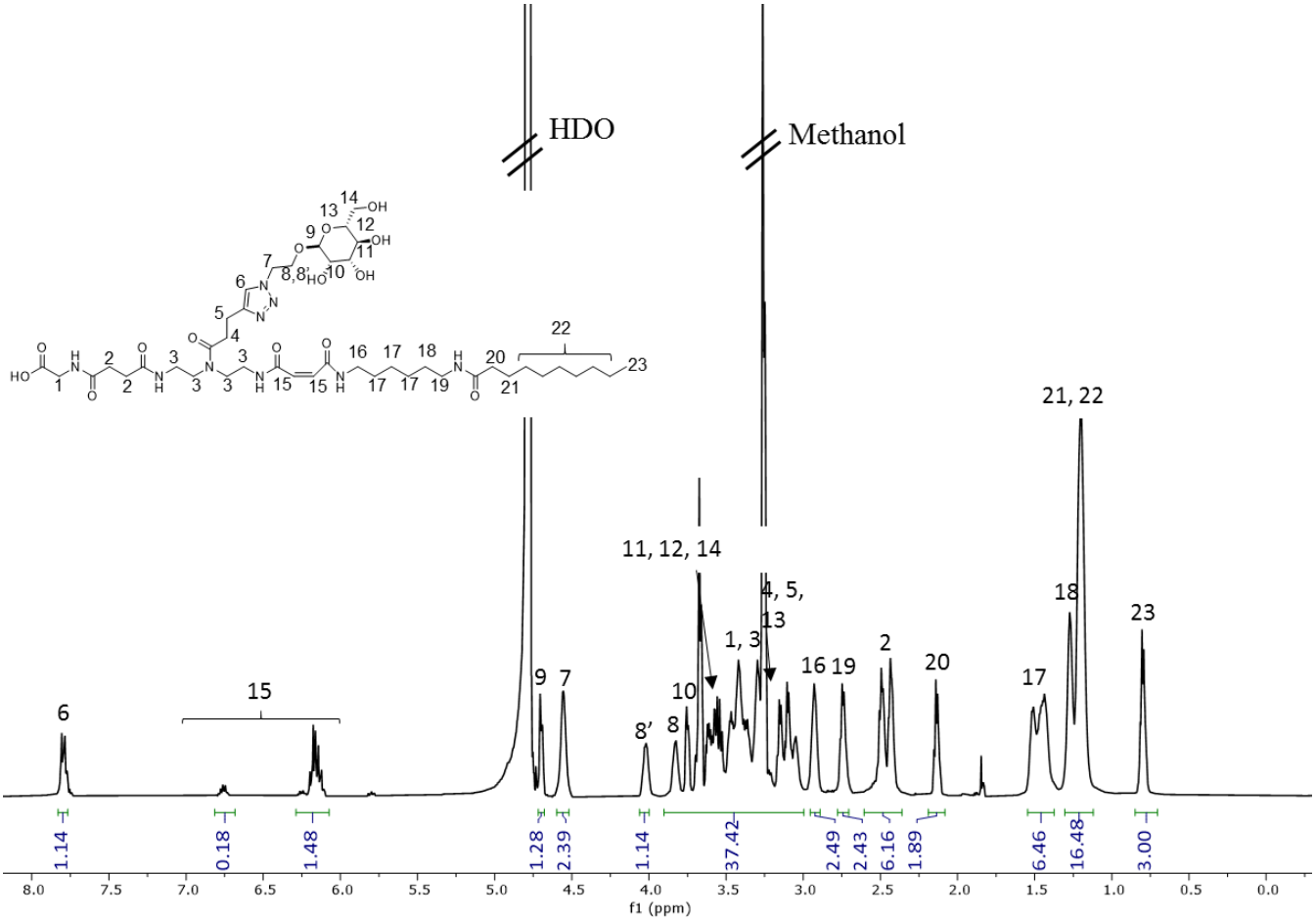

Figure S7. ^{1}H-NMR spectrum APG **2** recorded in D_2O/CD_3OD mixture. The individual protons are assigned by number.

^{1}H NMR (600 MHz, D_2O, CD_3OD): δ (ppm) 7.79 (m, 6), 6.76 – 6.04 (m, 15), 4.75 – 4.64 (m, 9), 4.61 – 4.44 (m, 7), 4.11 – 3.97 (m, 8'), 3.94 – 2.99, (m, 1, 3, 4, 5, 8, 10, 11, 12, 13, 14), 2.96 – 2.89 (m, 16), 2.82 – 2.67 (m, 19), 2.52 – 2.41 (m, 2), 2.19 – 2.09 (m, 20), 1.54 – 1.37 (m, 17), 1.30 – 1.12 (m, 18, 21, 22), 0.88 – 0.69 (m, 23).

HR-ESI-MS for $C_{45}H_{77}N_9O_{14}$. (Exact monoisotopic mass 939.5277): $[M+2H]^{2+}$ calcd. 470.7711, found 470.7715, mass accuracy -0.7 ppm.

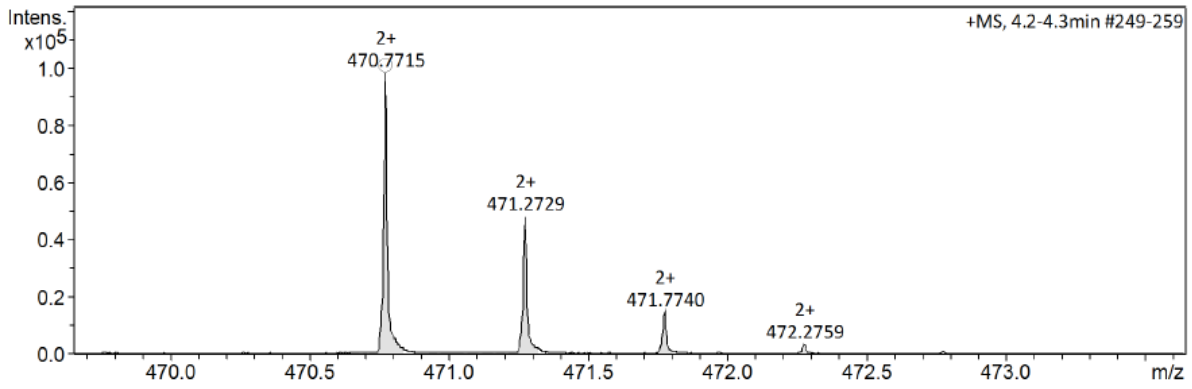

Figure S8. HR-ESI-MS of APG 2, recorded in positive mode.

RP-HPLC (linear gradient from 0 - 100% eluent B in 30 min at 25 °C): t_R = 14.25 min. Determined relative purity: >90% (Peak at t_r=14.25 and 14.65 have the same mass (data not shown) and are probably isomers caused by the HDM building block).

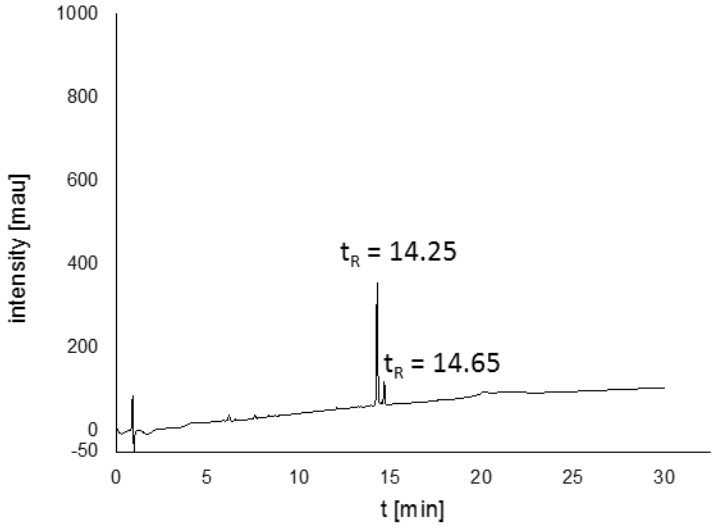

Figure S9. RP-HPLC of APG **2** (linear gradient from 5-95% acetonitrile in water in 30 min at 25°C).

APG **1**, Gly-TDS(MAN)-HDM-C12

The integral for the multiplets between 3.94 – 3.48 is larger than expected, due to a baseline increase which is derived through the self-assembly nature of the material. Furthermore, the integral for the alkene moiety of the HDM building block is decreased. Potentially this is due to the acidic nature of the alkene protons and that the protons are exchanged with deuterium, thus decreasing the integral. Additionally, this NMR measurement was performed at 50°C.

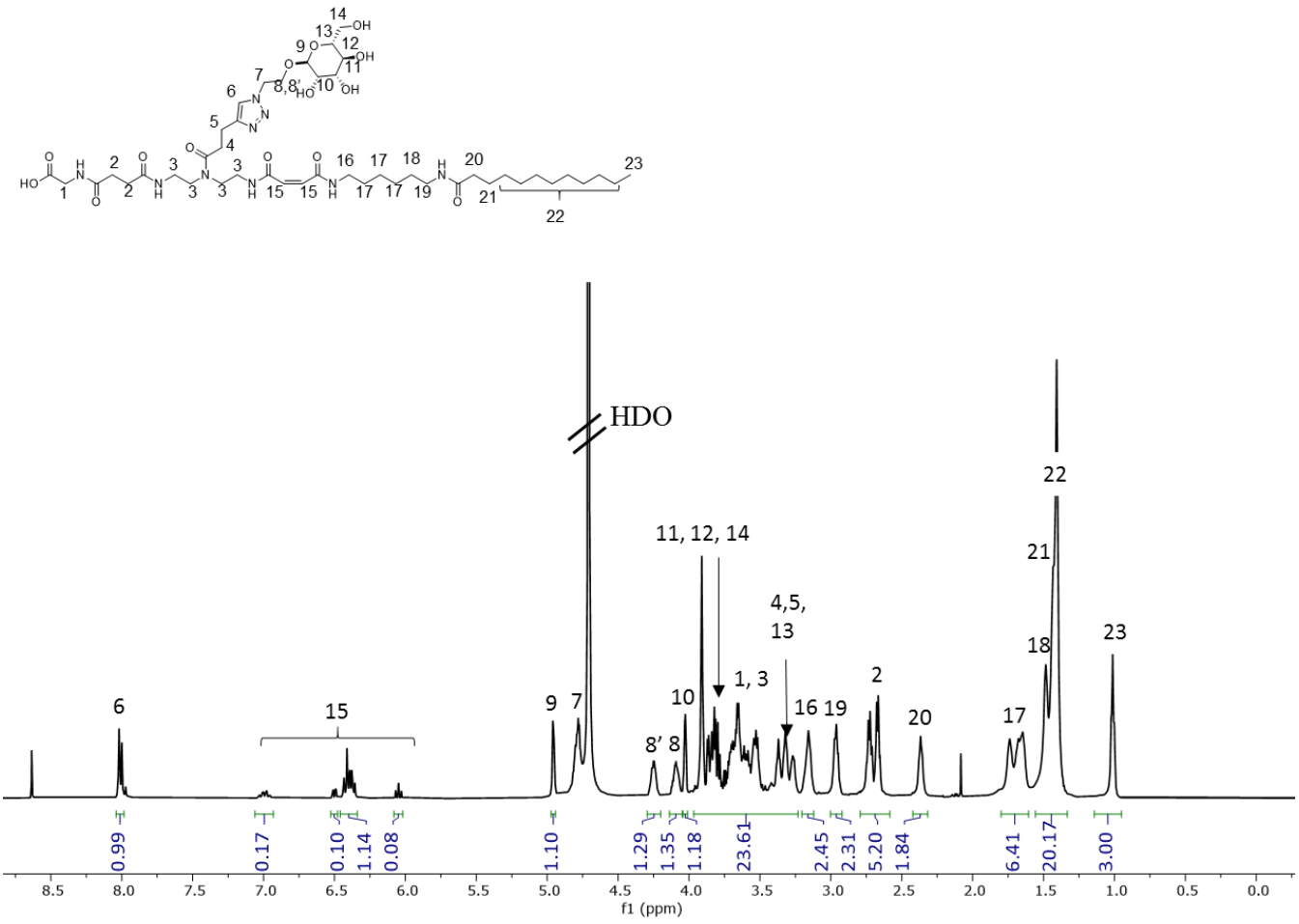

Figure S10. ^{1}H-NMR spectrum APG **1** recorded in D_2O. The individual protons are assigned by number.

^{1}H NMR (600 MHz, D_2O) δ 8.05 – 7.96 (m, 6), 7.05 – 6.02 (m, 15), 4.98 – 4.94 (m, 9), 4.83 – 4.74 (m, 7), 4.28 – 4.21 (m, 8'), 4.14 – 4.06 (m, 8), 4.06 – 4.01 (m, 10), 3.94 – 3.23 (m, 1, 3, 4, 5, 13, 11, 12, 14), 3.20 – 3.11 (m, 16), 3.01 – 2.91 (m, 19), 2.78 – 2.62 (m, 2), 2.41 – 2.32 (m, 20), 1.78 – 1.61 (m, 17), 1.54 – 1.38 (m, 18, 21, 22), 1.14 – 0.95 (m, 23).

HR-ESI-MS for $C_{45}H_{77}N_9O_{14}$. (Exact monoisotopic mass 967.5590): $[M+2H]^{2+}$ calcd. 484.7868, found 484.7872, mass accuracy -0.9 ppm.

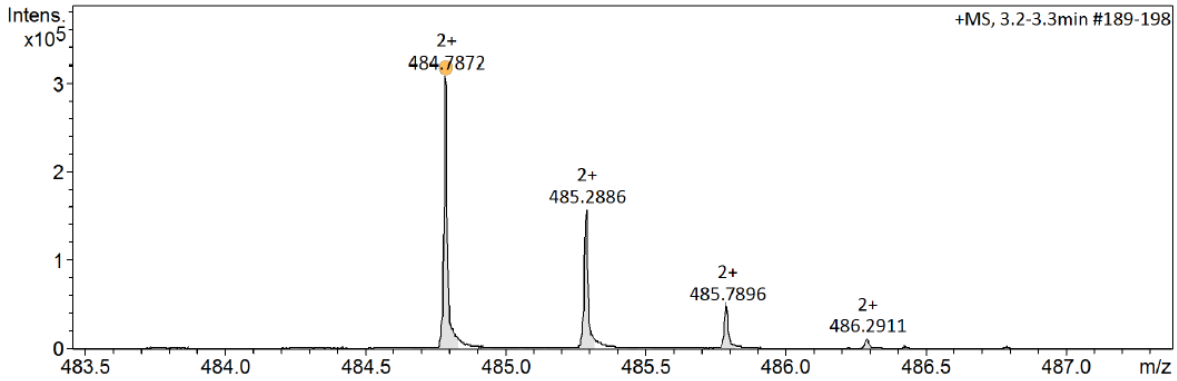

Figure S11. HR-ESI-MS of APG 1, recorded in positive mode.

RP-HPLC (linear gradient from 0 - 100% eluent B in 30 min at 25 °C): t_R = 17.0 min. Determined relative purity: >90% (Peak at t_r=17.0 and 17.3 have the same mass (data not shown) and are probably isomers caused by the HDM building block).

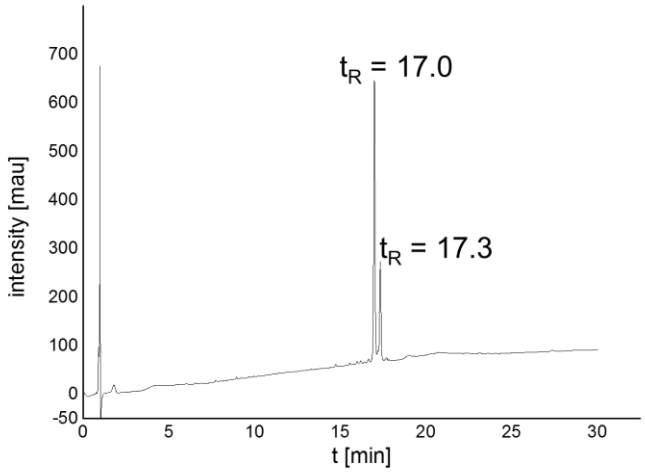

Figure S12. RP-HPLC of APG **1** (linear gradient from 5-95% acetonitrile in water in 30 min at 25°C).

APG **3**, Gly-TDS(MAN)-HDM-C15

The anomeric proton of Mannose (9) could not be integrated in ^{1}HNMR due to the overlaying signal from the residual water signal. An unidentified signal was detected with a chemical shift of δ 3.694 (s) ppm. The integral for the multiplets between 3.73 – 3.21 is larger than expected, due to a baseline increase which is derived through the self-assembly nature of the material. In order to suppress the baseline increase as much as possible a solvent mixture of D_2O and CD_3OD was used. Furthermore, the integral for the alkene moiety of the HDM building block is decreased. Potentially this is due to the acidic nature of the alkene protons and that the protons are exchanged with deuterium, thus decreasing the integral.

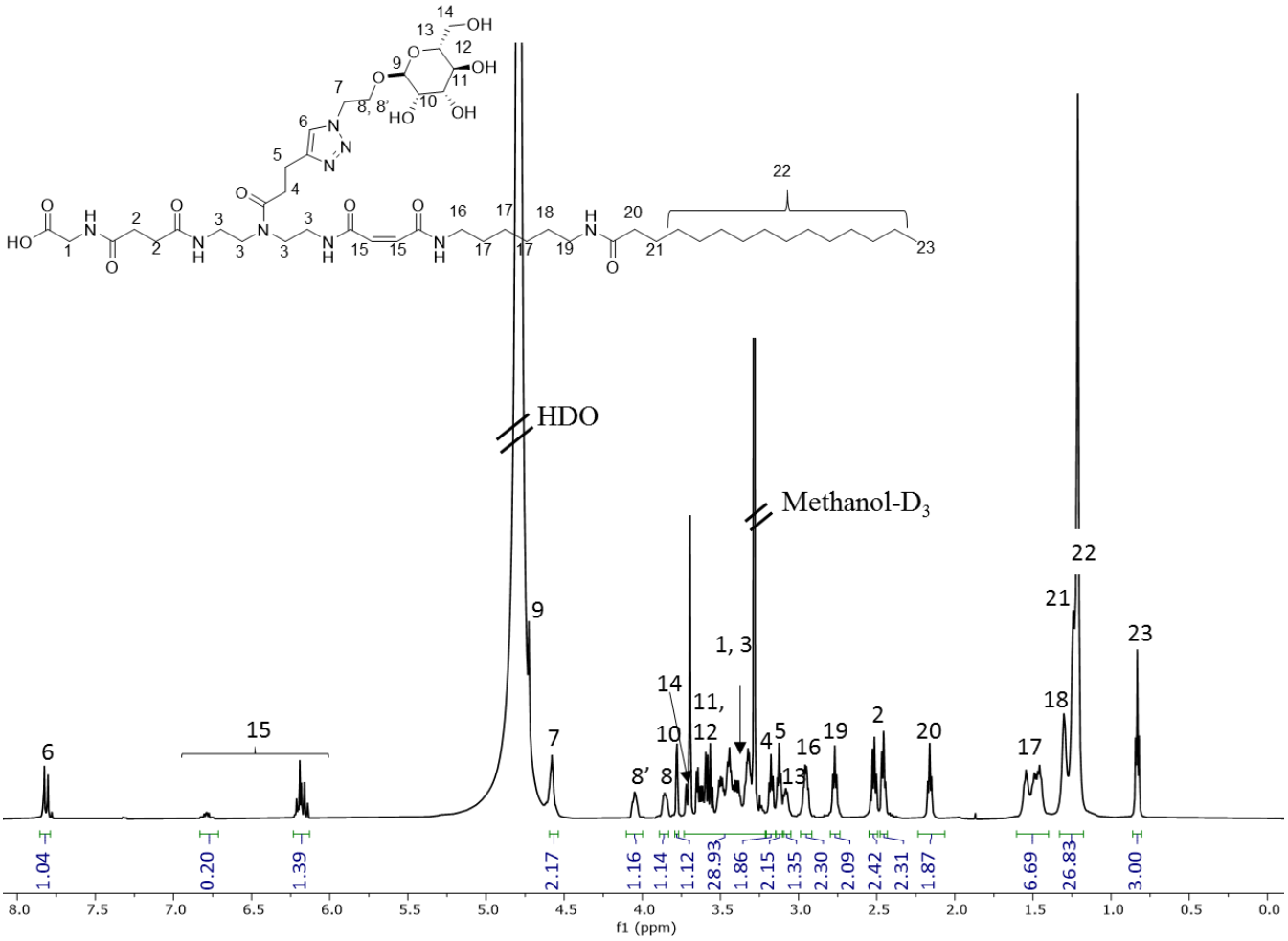

Figure S13. ^{1}H-NMR spectrum APG **3** recorded in D_2O/CD_3OD mixture. The individual protons are assigned by number.

^{1}H NMR (600 MHz, Deuterium Oxide, CD_3OD) δ 7.95 – 7.66 (m, 7), 6.8 – 6.13 (m, 15), 4.75 – 4.65 (m, 9), 4.61 – 4.53 (m, 7), 4.08 – 4.02 (m, 8'), 3.89 – 3.83 (m, 8), 3.80 – 3.76 (m, 10), 3.73 – 3.21 (m, 1, 3, 11, 12, 14), 3.18 (t, *J* = 7.1 Hz, 6), 3.12 (t, *J* = 6.8 Hz, 5), 3.10 – 3.05 (m, 1H, 13), 3.01 – 2.87 (m, 16), 2.77 (t, *J* = 7.4 Hz, 2H, 19), 2.58 – 2.39 (m, 2), 2.16 (t, *J* = 7.2 Hz, 20), 1.58 – 1.41 (m, 17), 1.34 – 1.17 (m, 18, 21, 22), 0.83 (t, *J* = 7.0 Hz, 23).

HR-ESI-MS for $C_{48}H_{83}N_9O_{14}$ (Exact monoisotopic mass 1009.6059): $[M+2H]^{2+}$ calcd. 505.8103, found 505.8101, mass accuracy 0.3 ppm.

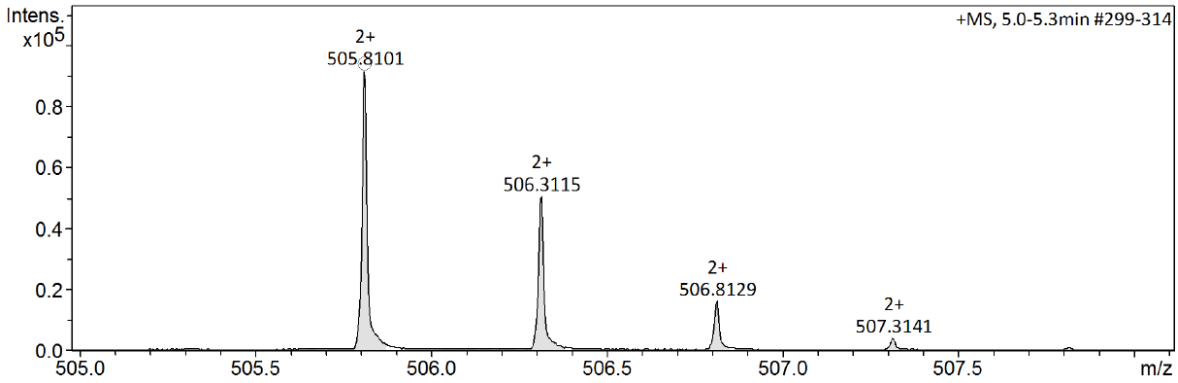

Figure S14. HR-ESI-MS of APG **3**, recorded in positive mode.

RP-HPLC (linear gradient from 0 - 100% eluent B in 30 min at 25 °C): t_r = 20.58. Determined relative purity: >90% (Peak at t_r=20.58 and 20.91 have the same mass (data not shown) and are probably isomers caused by the HDM building block).

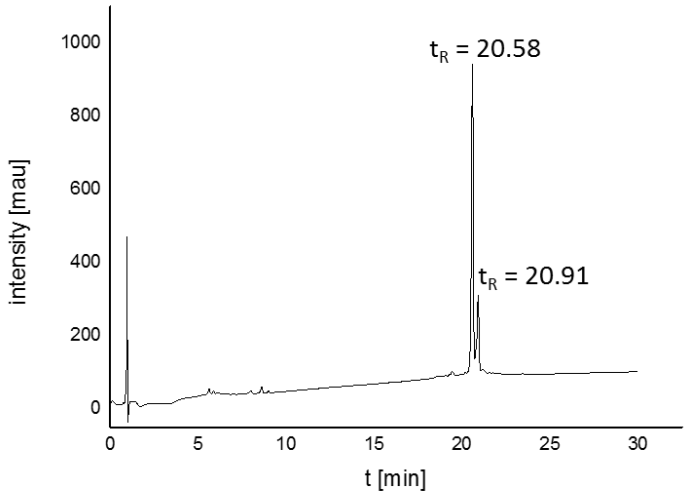

Figure S15. RP-HPLC of APG **3** (linear gradient from 5-95% acetonitrile in water in 30 min at 25°C).

APG **4**, Gly-TDS(Gal)-HDM-C12

The anomeric proton of Galactose (9) could not be integrated in ^{1}HNMR due to the overlaying signal from the residual water signal. In order to suppress the baseline increase as much as possible a solvent mixture of D_2O and CD_3OD was used. Furthermore, the integral for the alkene moiety of the HDM building block is decreased. Potentially this is due to the acidic nature of the alkene protons and that the protons are exchanged with deuterium, thus decreasing the integral.

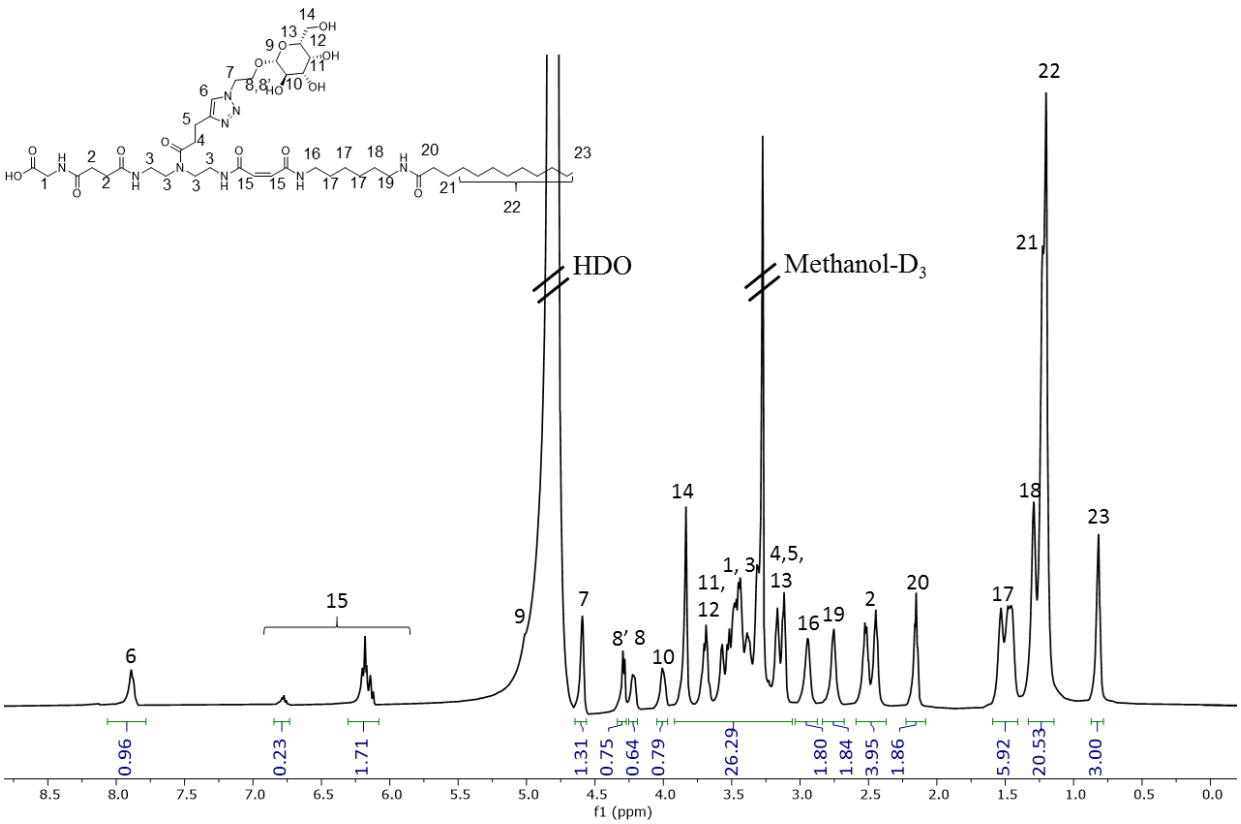

Figure S16. ^{1}H-NMR spectrum APG **4** recorded in D_2O/CD_3OD mixture. The individual protons are assigned by number.

^{1}H NMR (600 MHz, Deuterium Oxide, CD_3OD) δ 8.01 – 7.81 (m, 6), 6.86– 6.10 (m, 15), 4.65 – 4.55 (m, 7), 4.35 – 4.18 (m, 8', 8), 4.07 – 3.94 (m, 10), 3.90 – 3.07 (m, 1, 3, 4, 5, 11, 12, 13, 14), 3.03 – 2.87 (m, 16), 2.84 – 2.68 (m, 19), 2.59 – 2.37 (m, 2), 2.23 – 2.08 (m, 20), 1.59 – 1.41 (m, 17), 1.36 – 1.14 (m, 18, 21, 22), 0.82 (t, J = 6.9 Hz, 23).

HR-ESI-MS for $C_{45}H_{77}N_9O_{14}$ (Exact monoisotopic mass 967.5590): $[M+2H]^{2+}$ calcd. 484.7868, found 484.7872, mass accuracy -0.6 ppm.

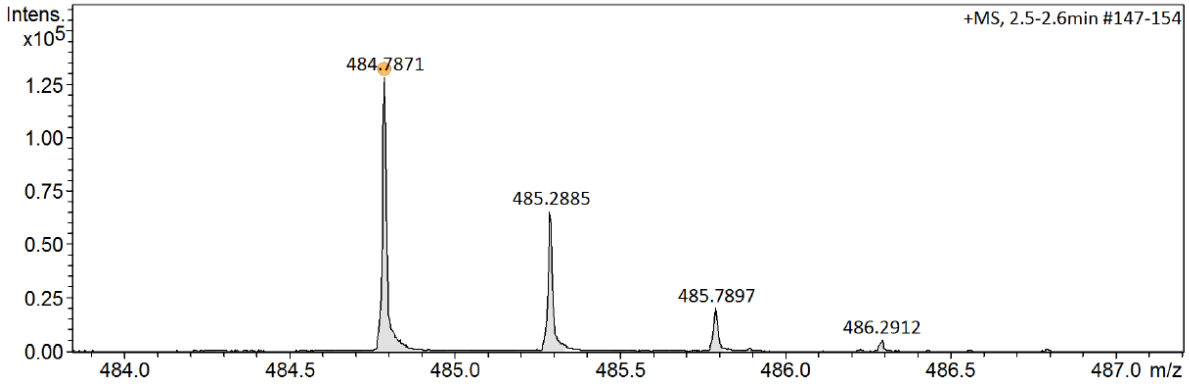

Figure S17. HR-ESI-MS of APG **4**, recorded in positive mode.

RP-HPLC (linear gradient from 0 - 100% eluent B in 30 min at 25 °C): t_R = 16.43 min. Determined relative purity: >90% (Peak at t_r=16.43 and 16.8 have the same mass (data not shown) and are probably isomers caused by the HDM building block).

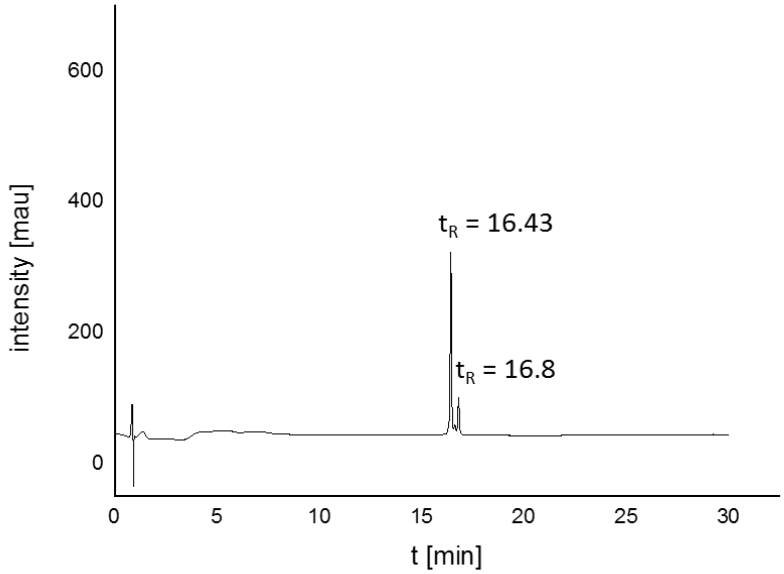

Figure S18. RP-HPLC of APG **4** (linear gradient from 5-95% acetonitrile in water in 30 min at 25°C).

APG **5**, TDS(Man)-HDM-C12

The anomeric proton of Mannose (9) could not be integrated in ^{1}HNMR due to the overlaying signal from the residual water signal. The same applies for signal 7. The integral for the multiplets between 4.03 – 3.30 is larger than expected, due to a baseline increase which is derived through the self-assembly nature of the material. In order to suppress the baseline increase as much as possible a solvent mixture of D_2O and CD_3OD was used. Furthermore, the integral for the alkene moiety of the HDM building block is decreased. Potentially this is due to the acidic nature of the alkene protons and that the protons are exchanged with deuterium, thus decreasing the integral.

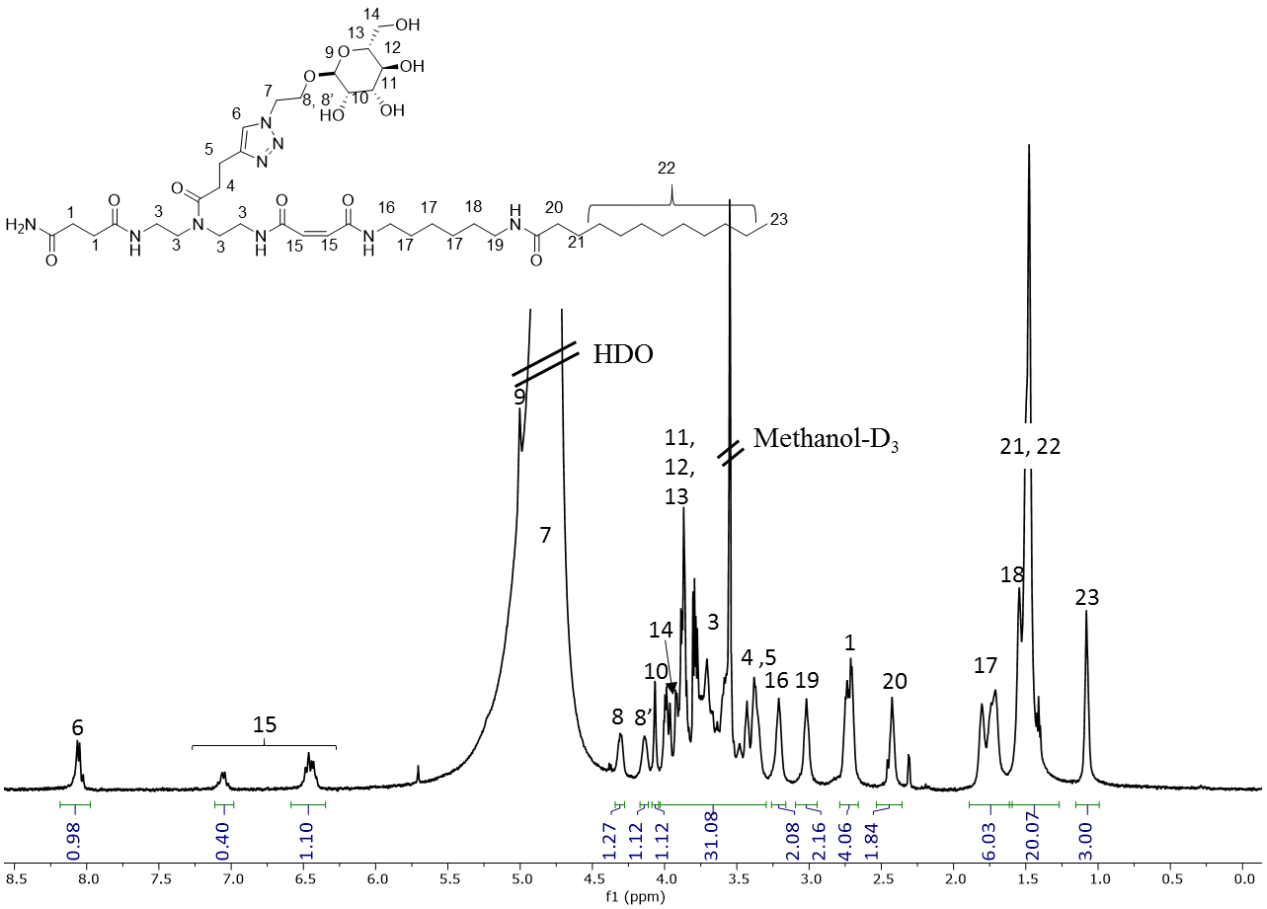

Figure S19. ^{1}H-NMR spectrum APG **5** recorded in D_2O/CD_3OD mixture. The individual protons are assigned by number.

^{1}H NMR (600 MHz, D_2O, CD_3OD) δ 8.12 – 8.00 (m, 6), 7.12 – 6.39 (m, 15), 4.37 – 4.28 (m, 1H, 8), 4.19 – 4.10 (m, 1H, 8'), 4.10 – 4.04 (m, 10), 4.03 – 3.3 (m, 3, 4, 5, 11, 12, 13, 14), 3.26 – 3.16 (m, 16), 3.07 – 2.95 (m, 19), 2.77 – 2.67 (m, 1), 2.51 – 2.38 (m, 20), 1.88 – 1.65 (m, 17), 1.60 – 1.33 (m, 18, 21, 22), 1.13 – 1.00 (m, 3H, 22).

HR-ESI-MS for $C_{43}H_{75}N_9O_{12}$ (Exact monoisotopic mass 909,5535): $[M+2H]^{2+}$ calcd. 455.7840, found 455.7845, mass accuracy -1.1 ppm.

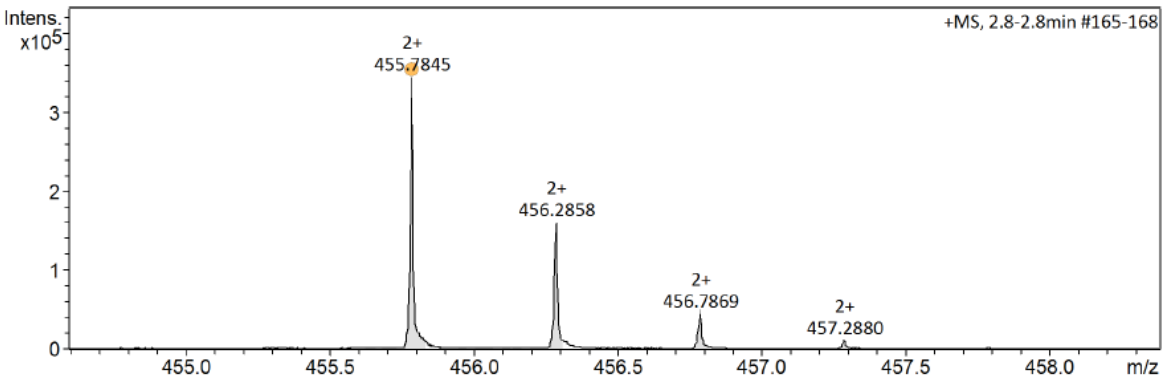

Figure S20. HR-ESI-MS of APG **5**, recorded in positive mode.

RP-HPLC (linear gradient from 0 - 100% eluent B in 30 min at 25 °C): t_r = 17.18. Determined relative purity: >90% (Peak at t_r=17.18 and 17.5 have the same mass (data not shown) and are probably isomers caused by the HDM building block).

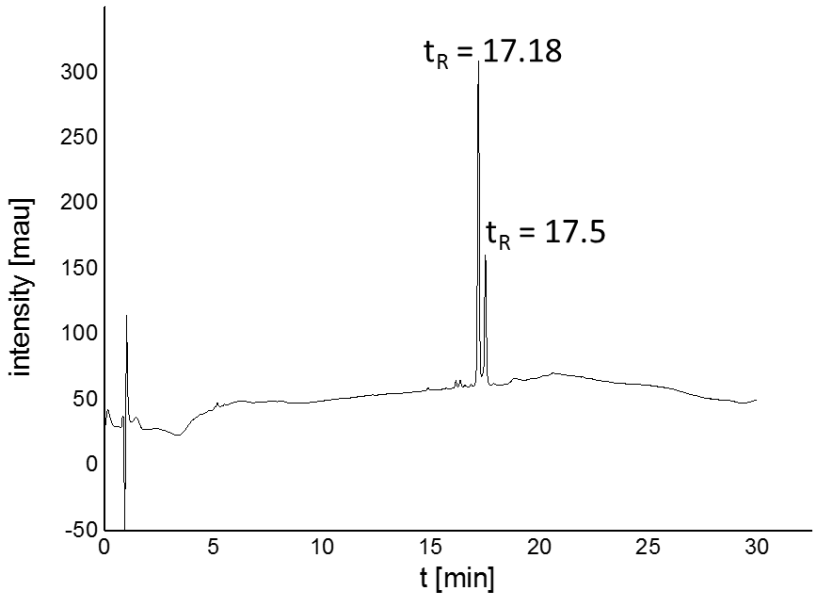

Figure S21. RP-HPLC of APG **5** (linear gradient from 5-95% acetonitrile in water in 30 min at 25°C).

APG **6**, Gly-TDS(Man)-HDS-C12

The anomeric proton of Mannose (9) could not be integrated in ^{1}HNMR due to the overlaying signal from the residual water signal. The integral for the multiplets between 3.97 – 3.32 is larger than expected, due to a baseline increase which is derived through the self-assembly nature of the material. In order to suppress the baseline increase as much as possible a solvent mixture of D_2O and CD_3OD was used.

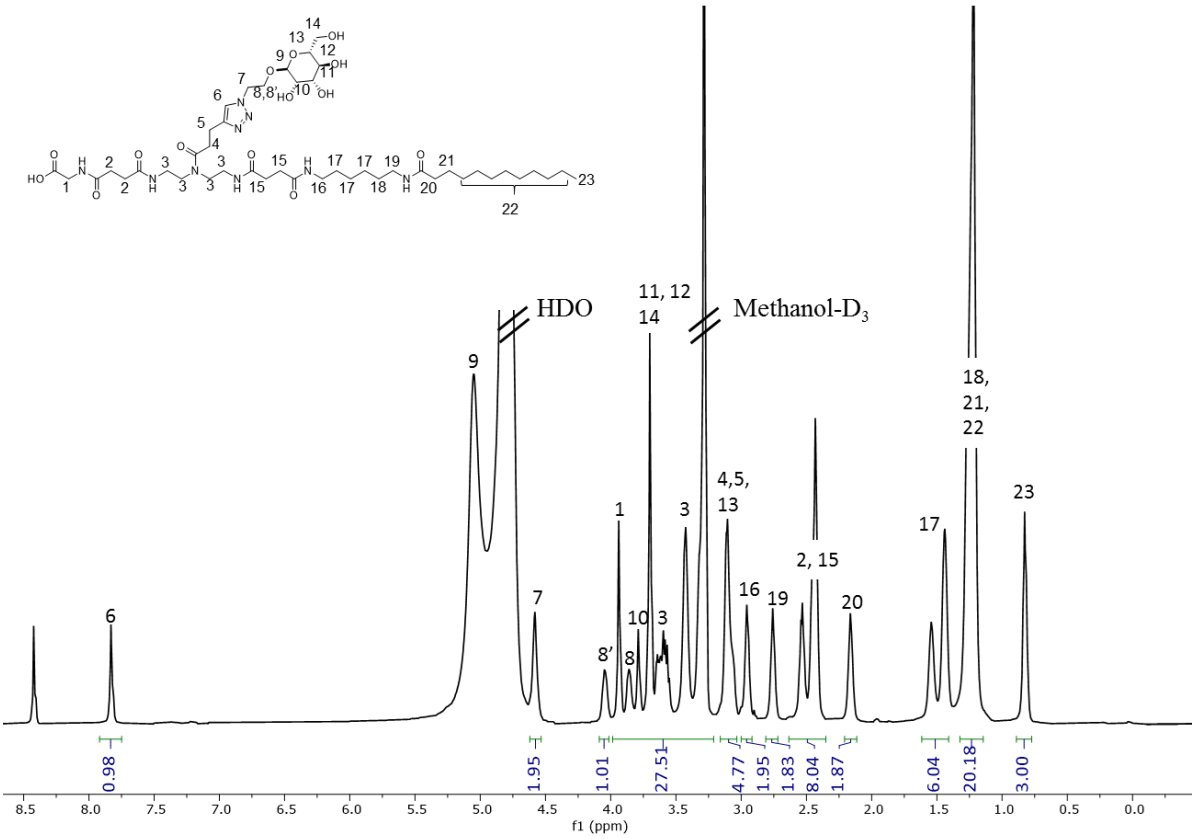

Figure S22. ^{1}H-NMR spectrum APG **6** recorded in D_2O/CD_3OD mixture. The individual protons are assigned by number.

^{1}H NMR (600 MHz, D_2O, CD_3OD) δ 7.86 – 7.80 (m, 6), 4.63 – 4.55 (m, 7), 4.08 – 4.01 (m, 8´), 3.97 – 3.32 (m, 1, 3, 10, 11, 12, 14), 3.15 – 3.04 (m, 4, 5, 13), 3.00 – 2.90 (m, 16), 2.83 – 2.66 (m,

19), 2.58 – 2.39 (m, 2, 15), 2.24 – 2.07 (m, 20), 1.61 – 1.37 (m, 17), 1.23 (m, 18, 21, 22), 0.89 – 0.75 (m, 23).

HR-ESI-MS for $C_{45}H_{79}N_9O_{14}$ (Exact monoisotopic mass 969,5746): $[M+2H]^{2+}$ calcd. 485.7946, found 485.7945, mass accuracy 0.1 ppm.

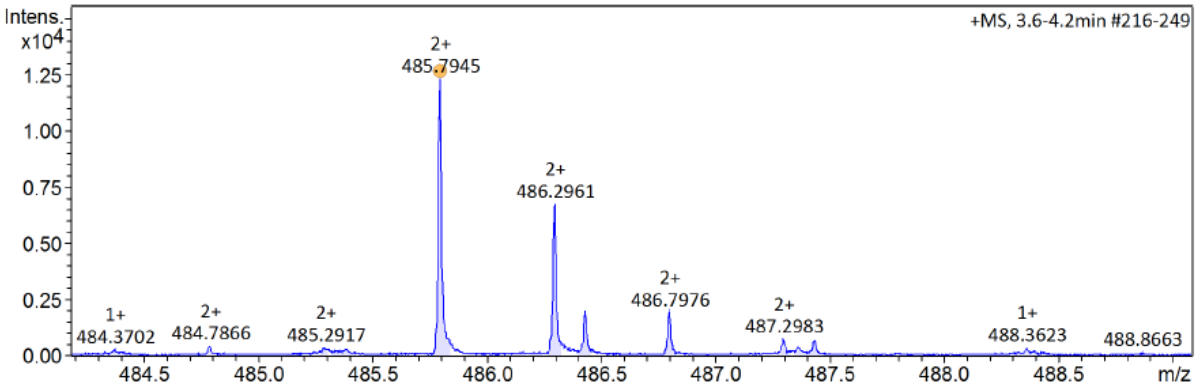

Figure S23. HR-ESI-MS of APG **6** recorded in positive mode

RP-HPLC (linear gradient from 0 - 100% eluent B in 30 min at 25 °C): t_R = 16.75 min. Determined relative purity: >90%.

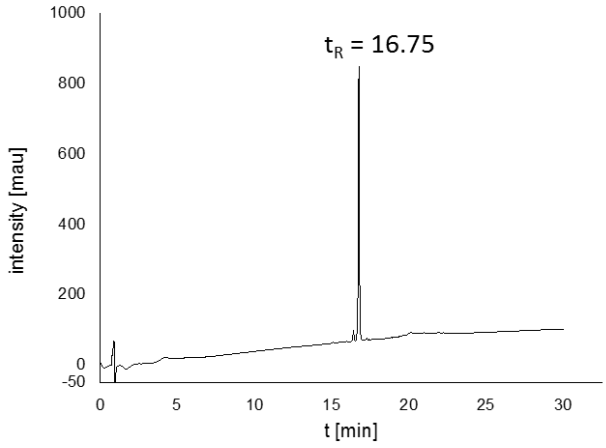

Figure S24. RP-HPLC of APG **6** (linear gradient from 5-95% acetonitrile in water in 30 min at 25°C).

APG **7,** TDS(Man)-C12

The anomeric proton of Mannose (9) could not be integrated in ^{1}HNMR due to the overlaying signal from the residual water signal. An unidentified signal was detected with a chemical shift of δ 5.42 (s) ppm. The integral for the multiple between 3.72 – 3.23 is larger than expected, due to a baseline increase which is derived through the self-assembly nature of the material and an overlap with the solvent signal. In order to suppress the baseline increase as much as possible a solvent mixture of D_2O and CD_3OD was used.

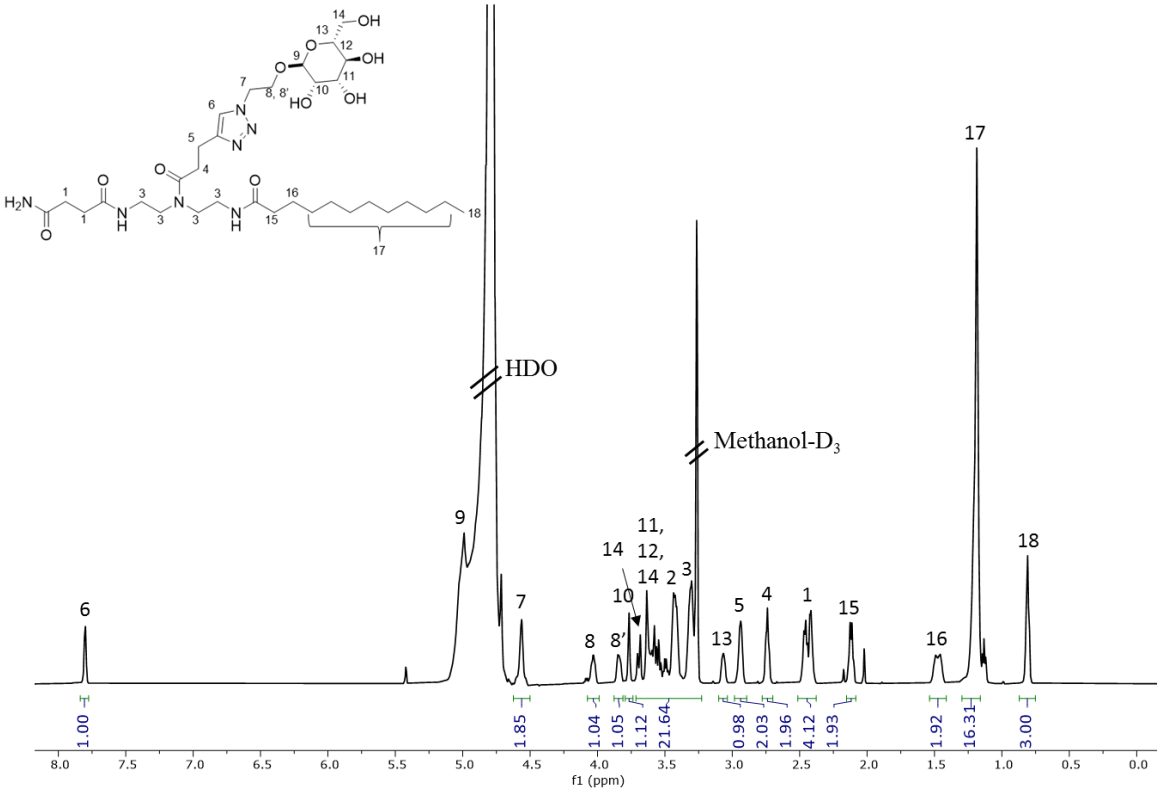

Figure S25. ^{1}H-NMR spectrum APG **7** recorded in D_2O/CD_3OD mixture. The individual protons are assigned by number.

^{1}H NMR (600 MHz, D_2O, CD_3OD) δ 7.83 – 7.78 (m, 6), 4.61 – 4.52 (m, 7), 4.08 – 4.00 (m, 8), 3.88 – 3.80 (m, 8'), 3.79 – 3.74 (m, 10), 3.72 – 3.23 (m, 2, 3, 10, 11, 12, 14), 3.09 – 3.05 (m, 13), 2.96 – 2.90 (m, 5), 2.74 (t, J = 7.4 Hz, 4), 2.51 – 2.33 (m, 1), 2.16 – 2.07 (m, 15), 1.56 – 1.41 (m, 16), 1.28 – 1.11 (m, 17), 0.87 – 0.75 (m, 18).

HR-ESI-MS for $C_{33}H_{59}N_7O_{10}$ (Exact monoisotopic mass 713.4323): $[M+H]^+$ calcd. 714.4396, found 714.4390, mass accuracy 0.8 ppm.

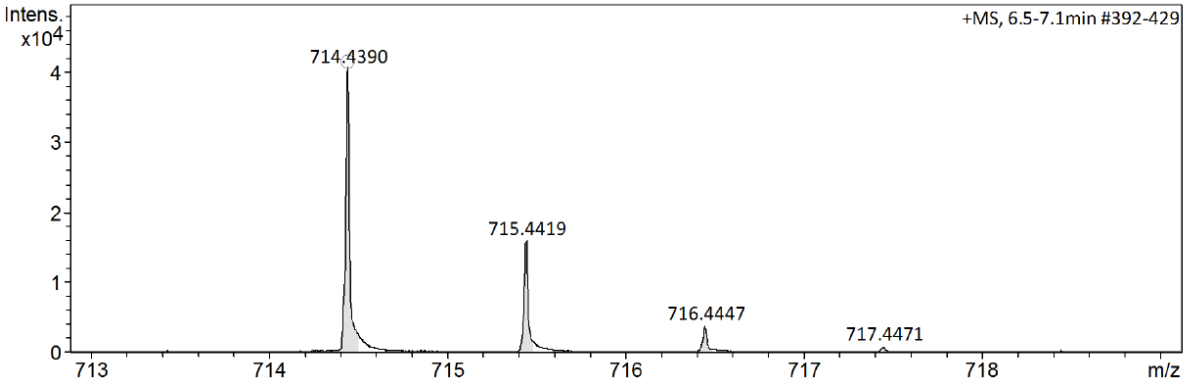

Figure S26. HR-ESI-MS of APG **7**, recorded in positive mode.

RP-HPLC (linear gradient from 0 - 100% eluent B in 30 min at 25 °C): tR = 15.71 min. Determined relative purity: >90%.

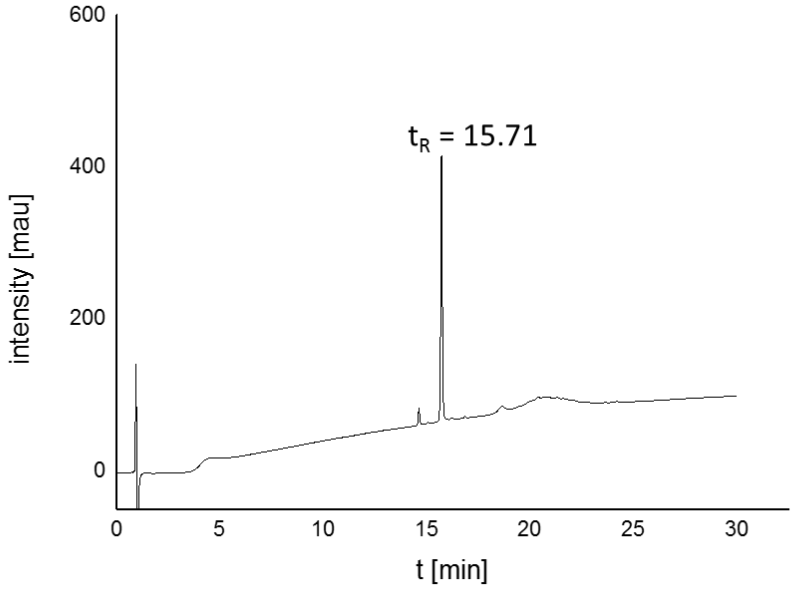

Figure S27. RP-HPLC of APG **7** (linear gradient from 5-95% acetonitrile in water in 30 min at 25°C).

APG **8**, Gly-BADS(Man)-HDM-C12

The anomeric proton of Mannose (8) could not be integrated in ^{1}HNMR due to the overlaying signal from the residual water signal. The integral for the multiple between 4.01 – 2.99 is larger than expected, due to a baseline increase which is derived through the self-assembly nature of the material. In order to suppress the baseline increase as much as possible a solvent mixture of D_2O and CD_3OD was used. Furthermore, the integral for the alkene moiety of the HDM building block is decreased. Potentially this is due to the acidic nature of the alkene protons and that the protons are exchanged with deuterium, thus decreasing the integral.

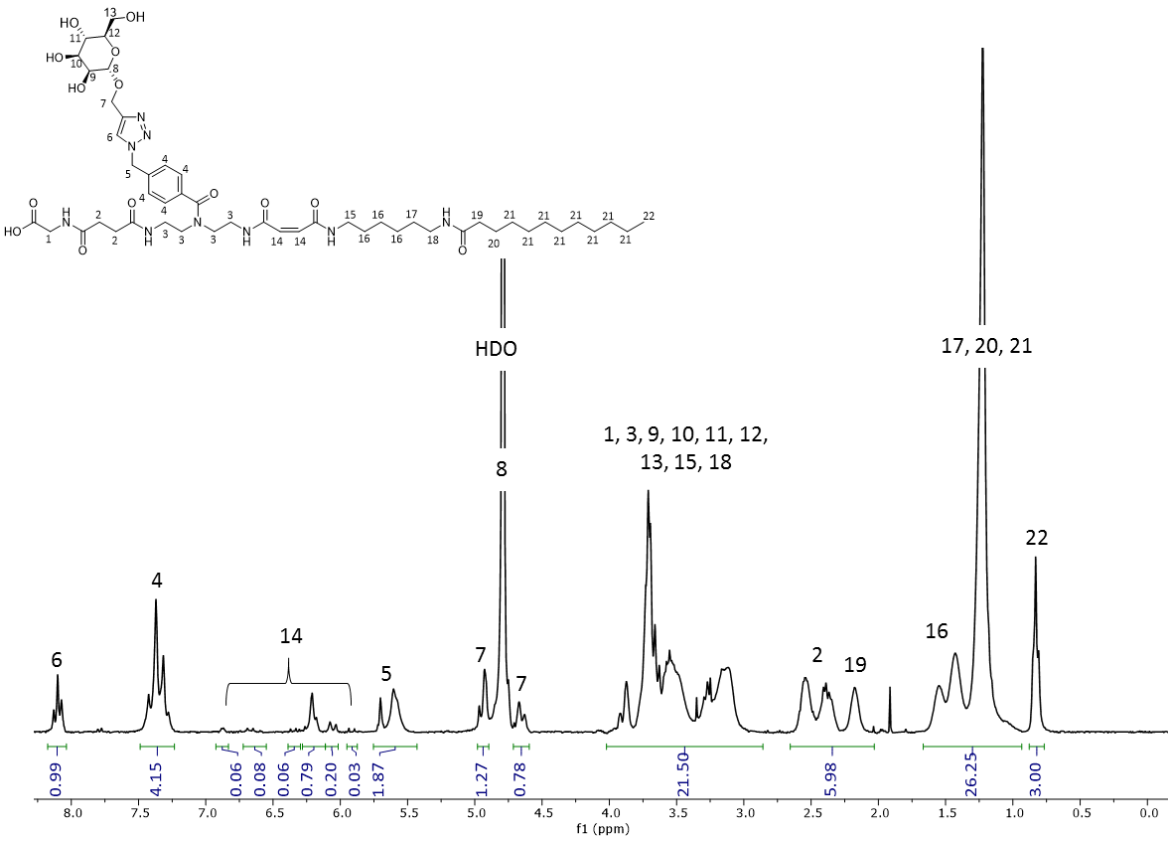

Figure S28. ^{1}H-NMR spectrum APG **8** recorded in D_2O/CD_3OD mixture. The individual protons are assigned by number.

^{1}H NMR (300 MHz, D_2O): δ (ppm) 8.17 – 8.03 (m, 6), 7.51 – 7.21 (m, 4), 6.89 – 5.85 (m, 14), 5.74 – 5.47 (m, 5), 4.99 – 4.89 (m, 7), 4.70 – 4.60 (m, 7), 4.01 – 2.99 (m, 1, 3, 9, 10, 11, 12, 13, 15, 18), 2.66 – 2.03 (m, 2, 20), 1.67 – 0.93 (m, 16, 17, 20, 21), 0.88 – 0.79 (m, 22).

HR-ESI-MS for $C_{49}H_{77}N_9O_{14}$. (Exact monoisotopic mass 1015,5590): $[M+2H]^{2+}$ calcd. 508.7868, found 508.7869, mass accuracy -0.2 ppm.

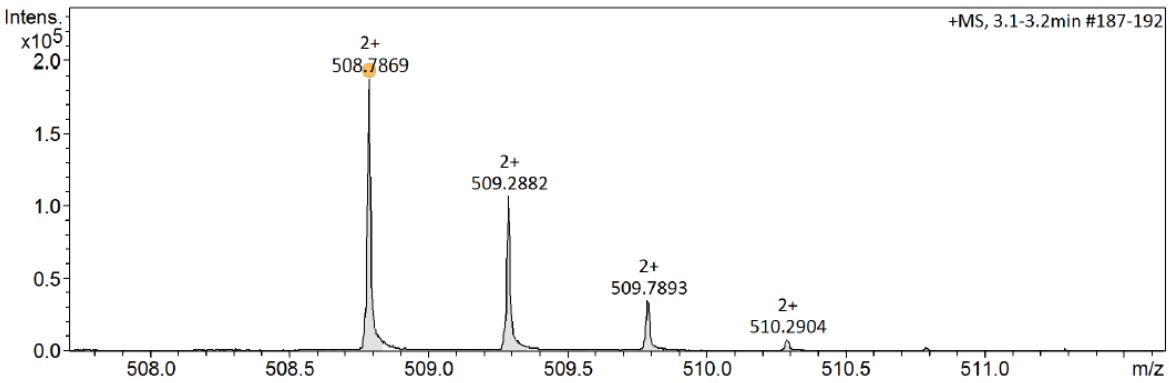

Figure S29. HR-ESI-MS of APG **8**, recorded in positive mode.

RP-HPLC (linear gradient from 0 - 100% eluent B in 30 min at 25 °C): t_r = 16.5. Determined relative purity: >90%.

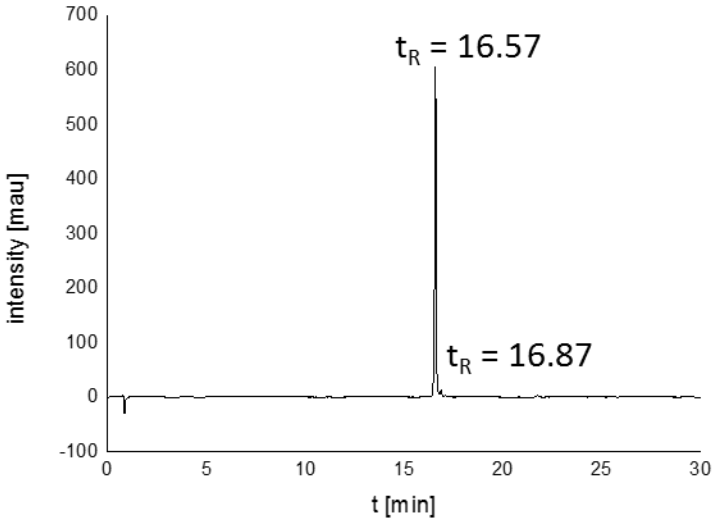

Figure S30. RP-HPLC of APG **8** (linear gradient from 5-95% acetonitrile in water in 30 min at 25°C).

3. Light scattering experiments

3.1 Dynamic light scattering

DLS measurements were performed in an angular range of 30 to 140° in 10°increments. At each angle three measurements were performed. All measurements were conducted at 25 °C. The concentration for the scattering experiments was 5 mM if not otherwise stated. Mean relaxation rates $\bar{\Gamma}$ were determined by applying the cumulant method. For the cumulant method the obtained autocorrelation functions were fitted using the equation below, which was derived by Frisken (see Equation 1).[4]

$$g^{(2)} = B + \beta * e^{-(2*\bar{\Gamma}*\tau)} * \left(1 + \frac{\mu_2}{2!} * \tau^2\right)^2 \quad (1)$$

$$with\ B = baseline, \beta = intercept, \bar{\Gamma} = \text{mean}\ relaxation\ rate, \tau = delay\ time\ and\ \mu_2 = second\ order\ cummulant$$

From this fit function the mean relaxation rate $\bar{\Gamma}$ can be derived. The relaxation rate is directly related to the diffusion coefficient D_t and to the squared scattering vector q.

$$D_t = \frac{\bar{\Gamma}}{q^2} \quad (2)$$

$$with\ D_t = translational\ diffusion\ coefficient, \bar{\Gamma} = \text{mean}\ relaxation\ rate\ and\ q = scattering\ vector$$

The magnitude of the scattering vector, q, is defined as:

$$q = \frac{4 * \pi * n}{\lambda_0} * \sin\left(\frac{\theta}{2}\right) \quad (3)$$

$$with\ n = refreactive\ index\ of\ the\ solvent, \lambda_0 = wavelength\ of\ the\ laser\ and$$

$$\theta = scattering\ angle$$

Using this relationship, the diffusion coefficient D_T can be determined. For that, the mean relaxation rate was plotted against the square of q and then the data points were fitted using a linear fit function. According to equation 2 the slope of the linear fit corresponds to the translational diffusion coefficient of the micelle samples. The Stokes-Einstein equation was applied to calculate the average hydrodynamic radius of the micelles.

$$R_H = \frac{k * T}{6 * \pi * \eta * D_T} \quad (4)$$

$$with\ R_H = hydrodynamic\ radius, k = \text{B}oltzmann\ constant, T = temperature\ and$$

$$\eta = viscosity$$

Table S3. Mean relaxation rates, squared vector and standard deviations for the DLS experiment of APG **1**, Gly-TDS(Man)-HDM-C12

Angle	q^2 [m^{-2}]	Mean relaxation rate $\bar{\Gamma}$ [s^{-1}]	Standard deviation [s^{-1}]
40	8.16×10^{13}	151	5
50	1.24×10^{14}	298	18
60	1.74×10^{14}	510	17
70	2.29×10^{14}	715	18
80	2.88×10^{14}	944	42
90	3.49×10^{14}	1244	18
100	4.09×10^{14}	1502	134
110	4.68×10^{14}	1722	25
120	5.23×10^{14}	2043	60
130	5.73×10^{14}	2211	42
140	6.16×10^{14}	2289	37

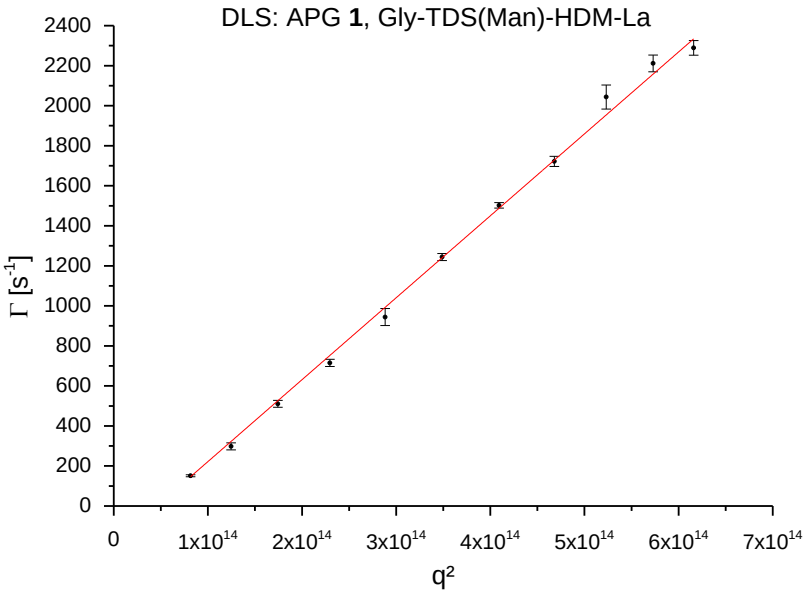

Figure S31. Linear fit of the plot from the relaxation rate against the squared scattering vector for APG **1**.

Table S4. Mean relaxation rates, squared vector and standard deviations for the DLS experiment of APG **6**, Gly-TDS(Man)-HDS-C12

Angle	q^2 [m^{-2}]	Mean relaxation rate $\bar{\Gamma}$ [s^{-1}]	Standard deviation [s^{-1}]
30	$4.67x10^{13}$	46	3
40	$8.16x10^{13}$	89	2
50	$1.24x10^{14}$	1645	17
60	$1.74x10^{14}$	248	10
70	$2.29x10^{14}$	371	16
80	$2.88x10^{14}$	477	13
90	$3.49x10^{14}$	605	245
100	$4.09x10^{14}$	697	3
110	$4.68x10^{14}$	812	15
120	$5.23x10^{14}$	919	19
130	$5.73x10^{14}$	1003	2
140	$6.16x10^{14}$	1051	4

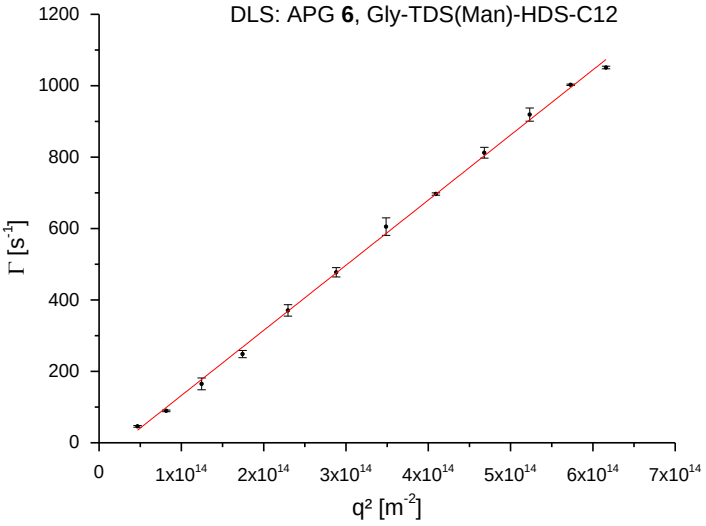

Figure S32. Linear fit of the plot from the relaxation rate against the squared scattering vector for APG **6.**

Table S5: Mean relaxation rates, squared vector and standard deviations for the DLS experiment of APG **7**, TDS(Man)-C12.

Angle	q^2 [m^{-2}]	Mean relaxation rate $\bar{\Gamma}$ [s^{-1}]	Standard deviation [s^{-1}]
30	$4.67x10^{13}$	49	5
40	$8.16x10^{13}$	115	11
50	$1.24x10^{14}$	203	19
60	$1.74x10^{14}$	337	28
70	$2.29x10^{14}$	558	9
80	$2.88x10^{14}$	644	18
90	$3.49x10^{14}$	898	43
100	$4.09x10^{14}$	1056	20
110	$4.68x10^{14}$	1194	84
120	$5.23x10^{14}$	1341	9
130	$5.73x10^{14}$	1432	43

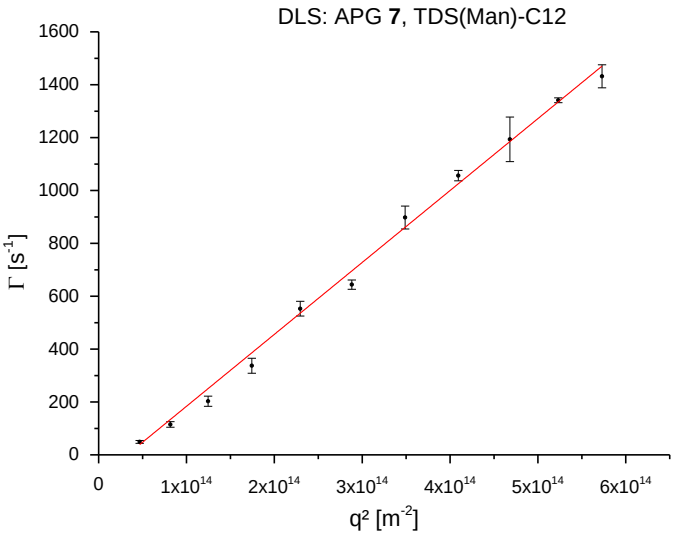

Figure S33. Linear fit of the plot from the relaxation rate against the squared scattering vector for APG **7.**

For APG **8** a concentration of 2.5 mM was used.

Table S6. Mean relaxation rates, squared vector and standard deviations for the DLS experiment of APG **8**, Gly-BADS(Man)-HDM-C12.

Angle	q^2 [m^{-2}]	Mean relaxation rate $\bar{\Gamma}$ [s^{-1}]	Standard deviation [s^{-1}]
40	$8.16x10^{13}$	186	3
50	$1.24x10^{14}$	286	5
60	$1.74x10^{14}$	432	3
70	$2.29x10^{14}$	589	12
80	$2.88x10^{14}$	789	5
90	$3.49x10^{14}$	969	6
100	$4.09x10^{14}$	1153	15
110	$4.68x10^{14}$	1336	19
120	$5.23x10^{14}$	1499	3
130	$5.73x10^{14}$	1615	15
140	$6.16x10^{14}$	1737	32

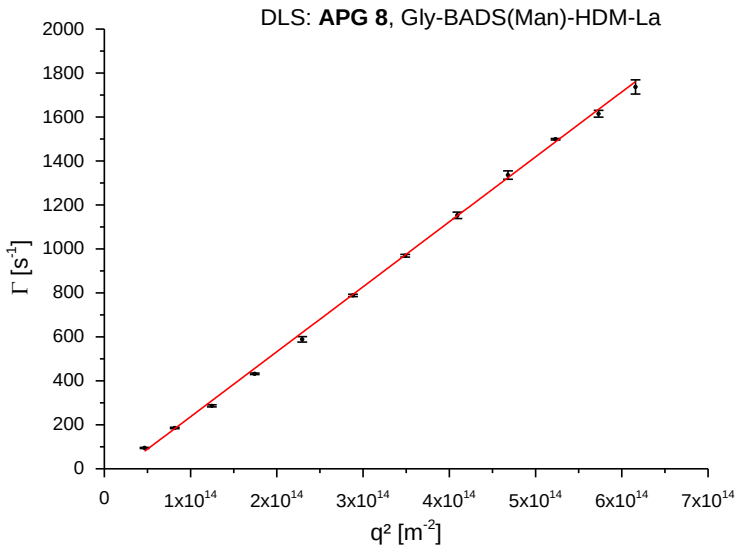

Figure S34. Linear fit of the plot from the relaxation rate against the squared scattering vector for APG **8.**

3.2 Dynamic depolarized light scattering

DDLS measurements were performed under the exact same conditions as mentioned before for DLS, except for the polarizer position in front of the detector, that was changed to crossed polarized (90°) conditions. The data obtained was processed as the DLS data and the obtained mean relaxation rates were again plotted against the square of q and the translational diffusion coefficients were obtained in the same manner as for DLS using the slopes of the respective linear fits to the data. While with the DLS data only the translational diffusion coefficient D_t could be determined, with the DDLS data the rotational diffusion coefficient D_r could be determined[5].

$$\bar{\Gamma} = D_t * q^2 + 6D_r \tag{5}$$

$$D_r = rotational\ diffusicon\ coefficient$$

Thus the intercept of the linear fit gives access to D_R. With the values for D_R and D_T at hand, the next step was the estimation of the dimensions of the micelles. Expecting cylindrical micelles, a theoretical approach from Garcia De la Torre *et al.* was followed in order to calculate the length and the radius of the micelles.[6-8] Garcia De la Torre *et al.* defined two functions of the axial ratio, which are shown in equation 6 and 7.

$$f(p) = \left(\frac{9 * \pi * \eta}{k * T}\right)^{\frac{2}{3}} * \frac{D_T}{(D_{R)})^{\frac{1}{3}}} \tag{6}$$

$$f(p) = \frac{\ln p + \upsilon}{(\ln p + \delta)^{\frac{1}{3}}} \tag{7}$$

$$with\ \eta = viscosity\ of\ the\ solvent, p = aspect\ ratio\ and$$

$$\upsilon\ and\ \delta = end - effect\ corrections\ depending\ on\ p$$

After f(p) was determined, the next step was the calculation of the axial ratio p (see Equation 8).

$$p = \frac{L}{2r} \tag{8}$$

$$with\ p = axial\ ratio, L = lenght\ and\ r = radius$$

Therefore, the numerical results for ν and δ, which have been calculated and regressed by Garcia De la Torre *et al.*, were used (see equation 9 and 10).[6, 7]

$$v = 0.312 + 0.565 * p^{-1} - 0.1 * p^{-2} \quad (9)$$

$$\delta = -0.662 + 0.917 * p^{-1} - 0.05 * p^{-2} \quad (10)$$

Equation 9 and 10 were inserted into equation 7 and the resulting final function was plotted as shown in Figure S 33.

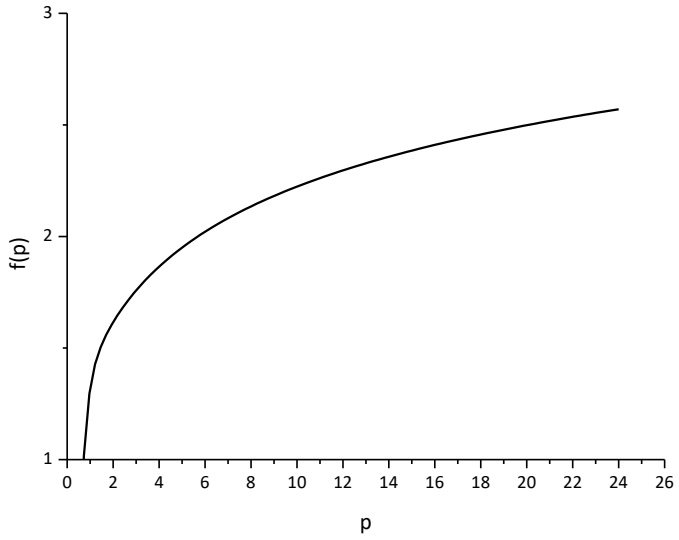

Figure S35. Plot of f(p) against the axial ratio p.

Using this plot p could be estimated. Using p and one of the equations 11 and 12, the length of the cylindrical micelles was calculated.[8]

$$L = \frac{(\ln p + 0.312 + 0.565 * p^{-1} - 0.1 * p^{-2}) * k * T}{3 * \pi * \eta * D_T} \quad (11)$$

$$L = \sqrt[3]{\frac{(\ln p - 0.662 + 0.917 * p^{-1} - 0.05 * p^{-2}) * k * T * 3}{\pi * \eta * D_R}} \quad (12)$$

$$with\ L = length\ of\ the\ rod$$

In the last step the radius of the rod was determined by using the axial ratio, which is given in equation 8.

Table S7. Mean relaxation rates, squared vector and standard deviations for the DDLS experiment of APG **6**, Gly-TDS(Man)-HDS-C12.

Angle	q^2 [m^{-2}]	Mean relaxation rate $\bar{\Gamma}$ [s^{-1}]	Standard deviation [s^{-1}]
30	4.67×10^{13}	143	28
40	8.16×10^{13}	215	2
50	1.24×10^{14}	269	15
60	1.74×10^{14}	341	7
70	2.29×10^{14}	376	8
80	2.88×10^{14}	470	24
90	3.49×10^{14}	534	8
100	4.09×10^{14}	705	7
110	4.68×10^{14}	733	3
120	5.23×10^{14}	827	22
130	5.73×10^{14}	872	21
140	6.16×10^{14}	884	32

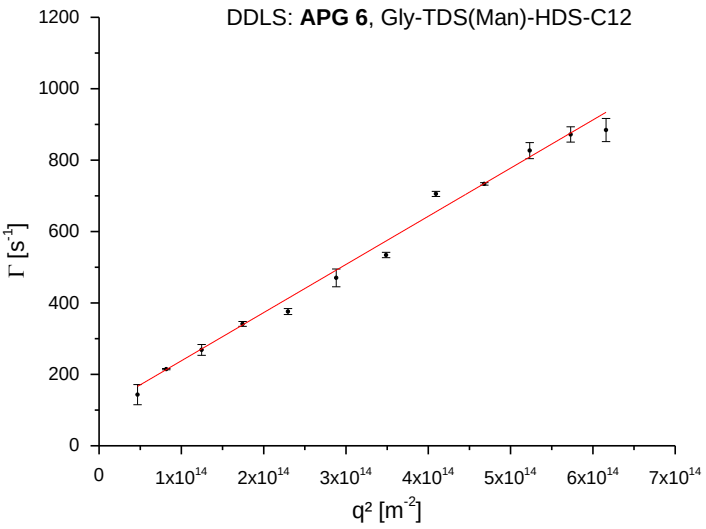

Figure S36. Linear fit of the plot from the relaxation rate against the squared scattering vector for APG **6.**

Table S8. Mean relaxation rates, squared vector and standard deviations for the DDLS experiment of APG **8**, Gly-BADS(Man)-HDM-C12.

Angle	q^2 [m^{-2}]	Mean relaxation rate $\bar{\Gamma}$ [s^{-1}]	Standard deviation [s^{-1}]
30	$4.67x10^{13}$	536	5
40	$8.16x10^{13}$	728	15
50	$1.24x10^{14}$	858	9
60	$1.74x10^{14}$	1027	46
70	$2.29x10^{14}$	1149	167
80	$2.88x10^{14}$	1238	42
90	$3.49x10^{14}$	1393	20
100	$4.09x10^{14}$	1476	49
110	$4.68x10^{14}$	1676	50
120	$5.23x10^{14}$	1691	46
130	$5.73x10^{14}$	1802	53
140	$6.16x10^{14}$	1806	32

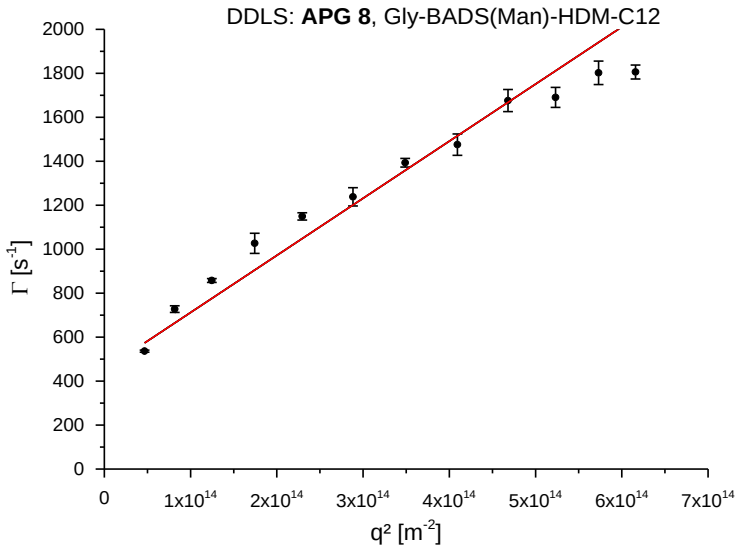

Figure S37. Linear fit of the plot from the relaxation rate against the squared scattering vector for APG **8.**

Table S9. Overview of the calculated values from the DLS and DDLS experiments for APG **6** and APG **8**.

Structure	D_T [m^2s^{-1}]	R_H [nm]	D_r [s^{-1}]	L [nm]	r [nm]
APG **6**	$1.59x10^{-12}$	160.5	15.5	888	56
APG **8**	$2.78x10^{-12}$	88.3	75.4	460	24

For TDS(Man)-C12 no signal could be detected in the depolarized setup, which indicates that isotropic (spherical) aggregates are formed.

For GLY-TDS(MAN)-HDM-C12 a signal was detected but the data could not be fitted, which indicates a high polydispersity.

4. Fluorescence spectroscopy

4.1.1 CMC determination with pyrene

For the fluorescence experiments a concentration series of the oligomers was prepared with a pyrene concentration of $2x10^{-6}$ mol/L in each sample. For that an acetone stock solution of pyrene was prepared with a concentration of $1.24x10^{-4}$ mol/L. In each vial 32.36 µl was pipetted and the acetone was allowed to evaporate. Then stock solutions of the oligomers were prepared and pipetted to the vials. Resulting in a concentration series with a constant pyrene concentration of $2x10^{-6}$ mol/l. The series was measured with a FLS980 Fluorometer from Edinburgh Instruments using following experimental conditions. Each sample was excited at 320 nm with a slit width of 5 mm and the fluorescence signal was collected between 350 and 450 nm in 0.4 nm steps. Every measurement was repeated 10 times to minimize errors.

Table S10. Results of the fluorescence pyrene probe experiment for APG **8**, Gly-BADS(Man)-HDM-C12.

Concentration [mmol/l]	APG **8**	I_1 at 372.5 nm	I_3 at 383 nm	I_3/I_1
0		8.58×10^{11}	4.44×10^{11}	0.52
0.10037		1.24×10^{12}	6.44×10^{11}	0.52
0.15056		1.12×10^{12}	6.17×10^{11}	0.55
0.20075		1.30×10^{12}	7.53×10^{11}	0.58
0.25093		1.08×10^{12}	6.33×10^{11}	0.59
0.30112		1.06×10^{12}	6.24×10^{11}	0.59
0.50187		1.12×10^{12}	7.46×10^{11}	0.67
0.7528		7.74×10^{11}	5.52×10^{11}	0.71
1.00374		8.93×10^{11}	6.92×10^{11}	0.78

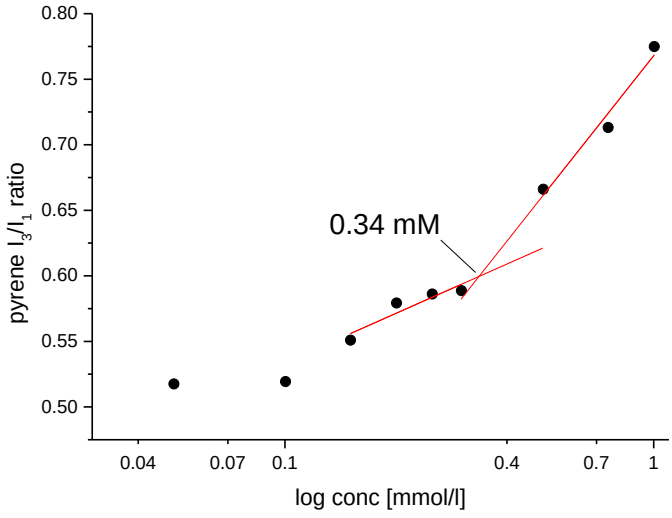

Figure S38. Pyrene I_3/I_1 ratio plotted against the logarithmic concentration of APG **8**.

Table S11. Results of the fluorescence pyrene probe experiment for APG **1**, Gly-TDS(Man)-HDM-C12.

Concentration [mmol/l]	APG **1** I_1 at 372.5 nm	I_3 at 383 nm	I_3/I_1
0	$1.52x10^{12}$	$8.2x10^{11}$	0.54
0.28	$4.84x10^{12}$	$2.6x10^{12}$	0.54
0.31	$3.6x10^{12}$	$1.93x10^{12}$	0.54
0.34	$5.13x10^{12}$	$2.76x10^{12}$	0.54
0.52	$4.22x10^{12}$	$2.27x10^{12}$	0.54
0.69	$1.66x10^{12}$	$9.66x10^{11}$	0.58
0.86	$2.63x10^{12}$	$1.48x10^{12}$	0.56
1.03	$2.25x10^{12}$	$1.27x10^{12}$	0.56
1.72	$2.16x10^{12}$	$1.57x10^{12}$	0.73
3.45	$7.45x10^{11}$	$5.42x10^{11}$	0.73

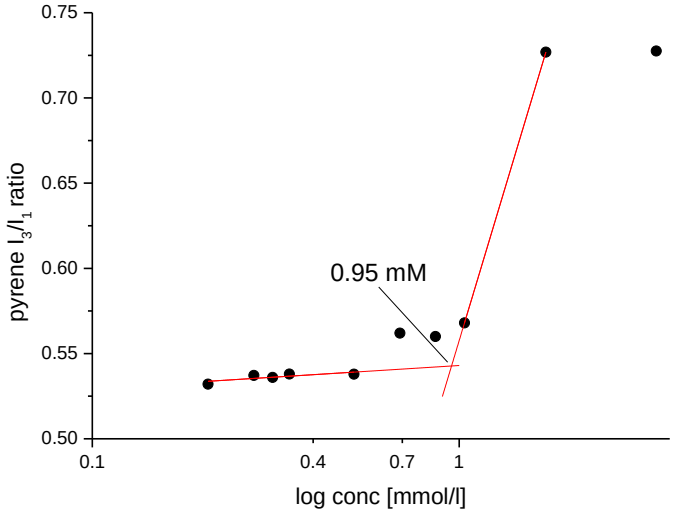

Figure S39. Pyrene I_3/I_1 ratio plotted against the logarithmic concentration of APG **1**.

Table S12. Results of the fluorescence pyrene probe experiment for APG **4**, Gly-TDS(Gal)-HDM-C12.

Concentration APG **4** [mol/l]	I_1 at 372.5 nm	I_3 at 383 nm	I_3/I_1
0.16	33716	18614	0.55
0.19	31432	18079	0.58
0.28	36492	21357	0.59
0.31	42307	24568	0.58
0.47	37357	22485	0.60
0.62	28899	18575	0.64
0.78	35314	22565	0.64
1.55	18835	16461	0.87
3.1	16624	14054	0.85

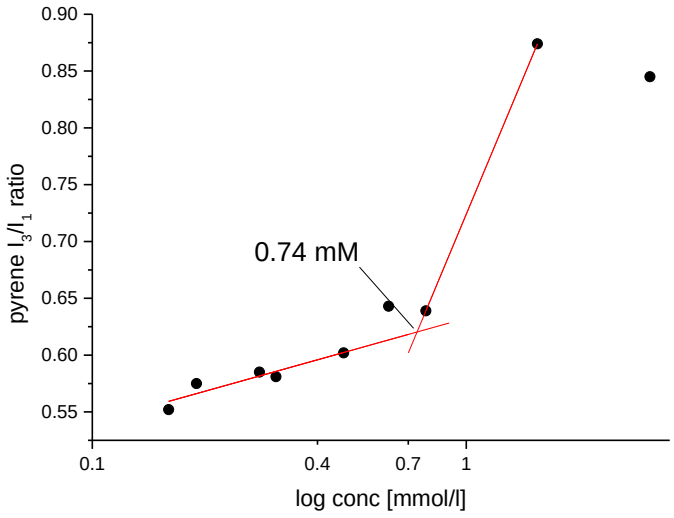

Figure S40. Pyrene I_3/I_1 ratio plotted against the logarithmic concentration of APG **4**.

4.1.2 Fluorescence overlap of APGs and pyrene

Fluorescence emission of pyrene and APGs overlap and requires background corrections.

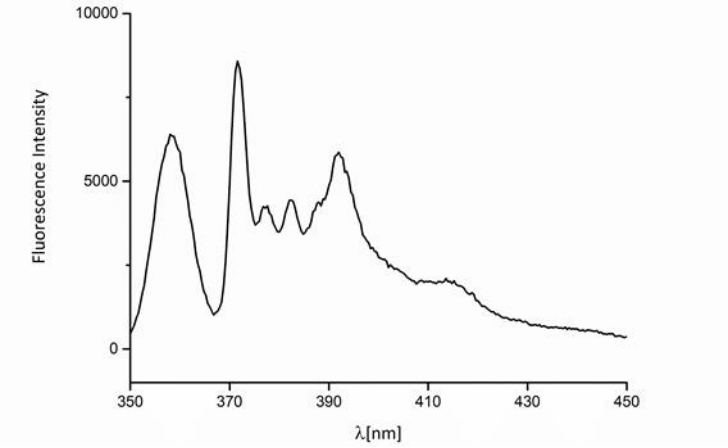

Figure S41. Pyrene fluorescence emission spectrum (ex. 320 nm).

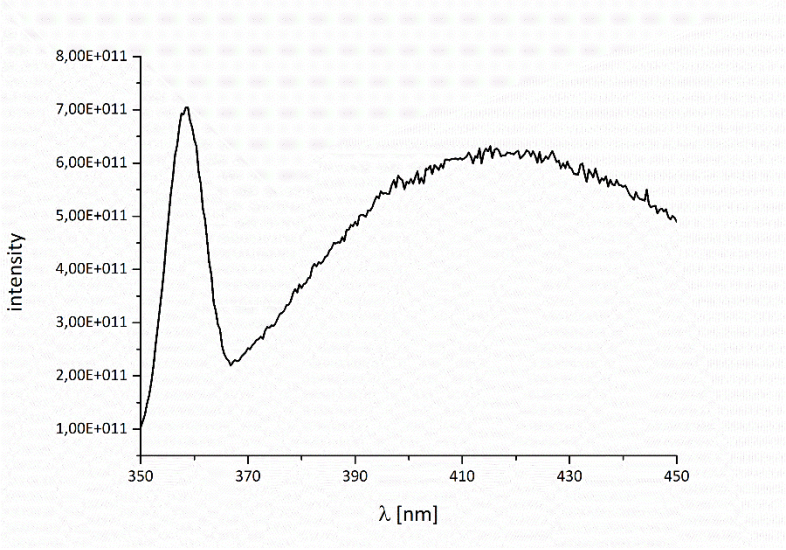

Figure S42. APG **8** fluorescence emission spectrum (ex. 320 nm).

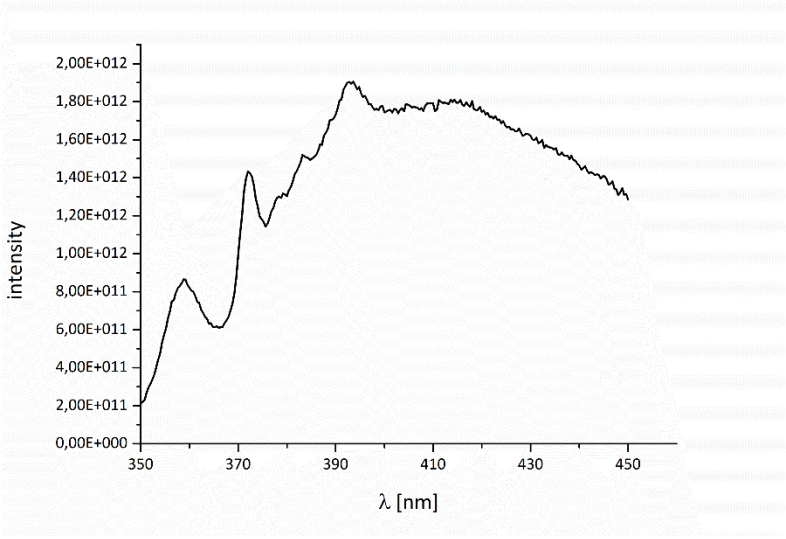

Figure S43. Combined APG **8** and pyrene fluorescence emission spectrum.

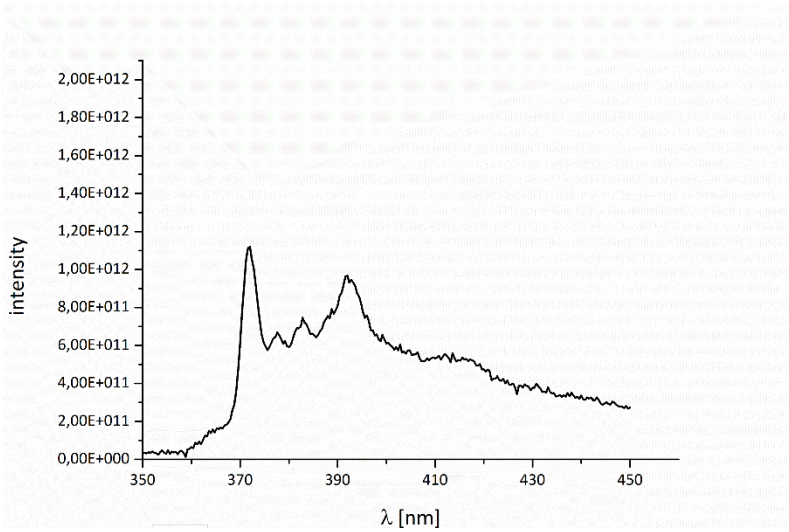

Figure S44. Fluorescence spectrum of APG8 and pyrene substracted by the spectrum of free APG8.

4.2 CMC determination with Nile red

Nile red is highly solvatochromic and can be excited at 550 nm. At this excitation wavelength the emission of the APGs is close to zero.

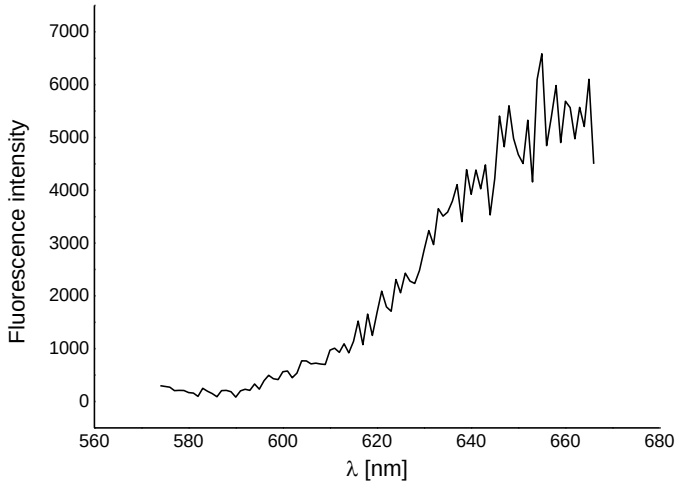

Figure S45. Fluorescence emission spectrum of nile red in water (ex. 550 nm).

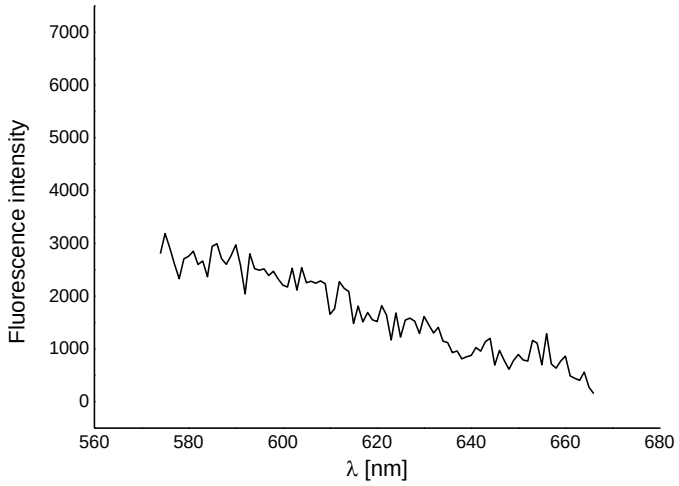

Figure S46. Fluorescence emission spectrum of APG 8 in water (ex. 550 nm).

For the fluorescence experiments a concentration series of the oligomers was prepared with a nile red concentration of $1x10^{-6}$ mol/L in each sample. For that a dioxane stock solution of nile red was prepared with a concentration of 0.129 mg/ml. Then in a glass tube 50 µl of the stock solution was pipetted into 10 ml of ultrapure water. A concentration series was prepared with a total volume of 100 µl in well plates. The series was measured with a Clariostar plate reader reader from BMG Labtech. Each sample was excited at λ_{ex} = 550 nm and data was collected at 635 nm. The measurements were performed in triplicates.

Table S13. CMC with nile red of APG **2**, GLY-TDS(MAN)-HDM-C10 CMC.

Concentration [mM]	Ø Counts @635 nm	Standard deviation
0.5	18323	2736
1	20687	1066
2	21483	2497
4	47618	1954
6	95131	7929
8	147263	12496
10	185969	6554

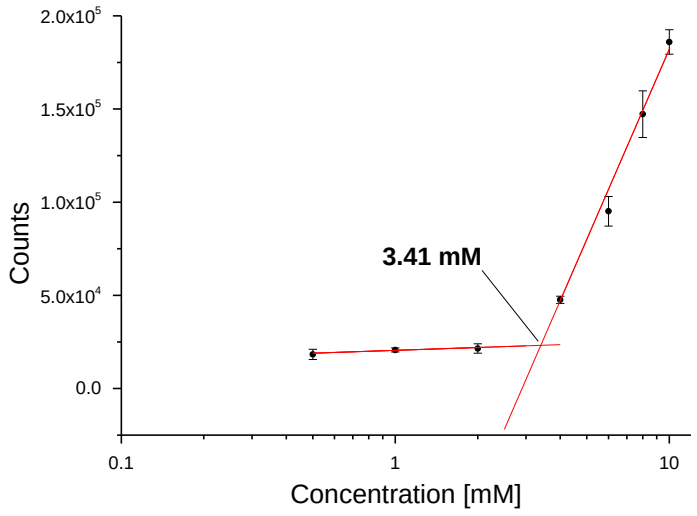

Figure S47. Counts plotted against the logarithmic concentration of APG **2**.

Table S14. CMC with nile red of APG **1**, GLY-TDS(MAN)-HDM-C12.

Concentration [mM]	Ø Counts @635 nm	Standard deviation
0	1753	491
0.1	2999	138
0.15	3290	291
0.25	5339	67
0.5	9869	12
0.75	18303	531
1	25358	1493
1.5	39092	487
2	52740	347
3	68528	218
4	72443	180

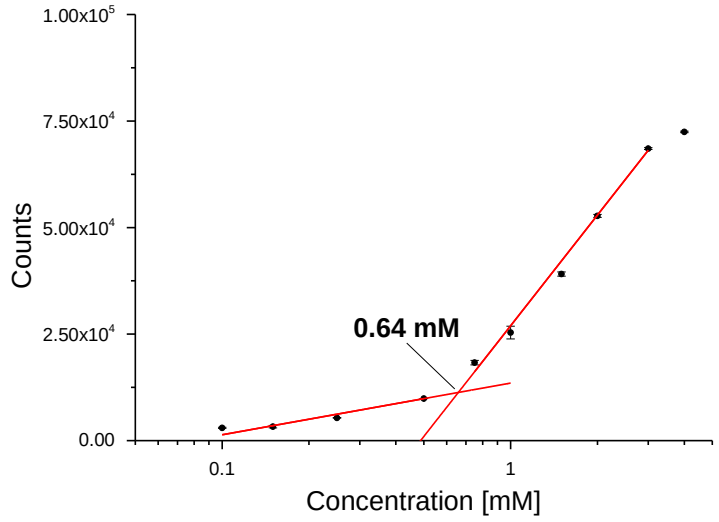

Figure S48. Counts plotted against the logarithmic concentration of APG **1**.

Table S15: CMC with nile red of APG **3**, GLY-TDS(MAN)-HDM-C15.

Concentration [mM]	Ø Counts @635 nm	Standard deviation
0	3407	578
0.02	4230	125
0.04	5933	1.5
0.06	7373	409
0.08	8923	714
0.1	12809	472
0.15	15966	3108
0.25	47026	1311
0.5	135363	12758
0.75	185388	8189
1	197668	11227
1.5	208685	605
2	226966	5175
3	229697	424
4	235331	343

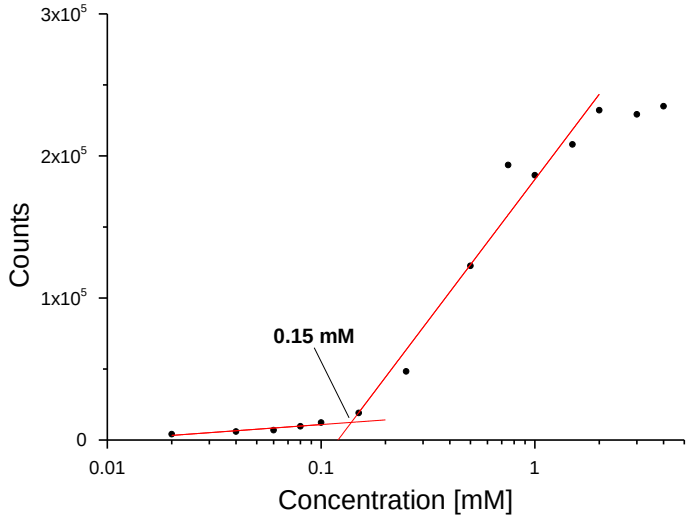

Figure S49. Counts plotted against the logarithmic concentration of APG **3**.

Table S16. CMC with nile red of APG **4**, GLY-TDS(Gal)-HDM-C12.

Concentration [mM]	Ø Counts @635 nm	Standard deviation
0	1160	23
0.1	2383	63
0.15	2268	111
0.25	3093	49
0.5	5077	69
0.75	9882	17
1	12691	73
1.5	21462	5
2	29667	149
3	45193	1379

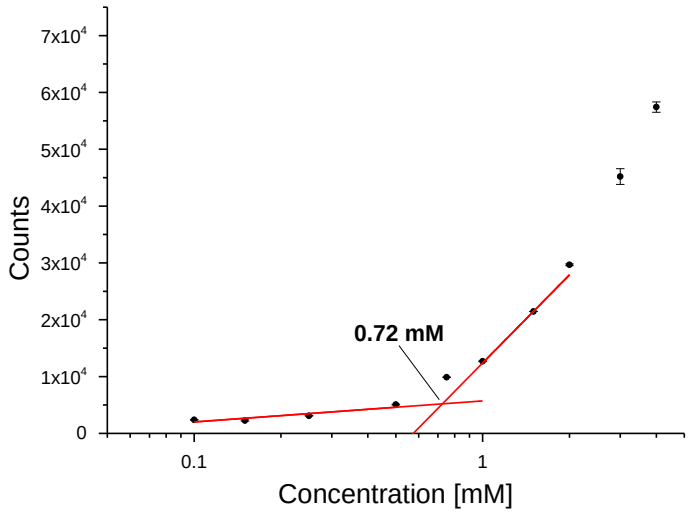

Figure S50. Counts plotted against the logarithmic concentration of APG **4**.

Table S17. CMC with nile red of APG **6**, Gly-TDS(Man)-HDS-C12.

Concentration [mM]	Ø Counts @635 nm	Standard deviation
0.1	5514	272
0.15	5422	201
0.25	6346	512
0.5	8667	143
0.75	10312	73
1	14580	199
1.5	22448	1235
2	39316	440
3	181688	868
4	239964	10647

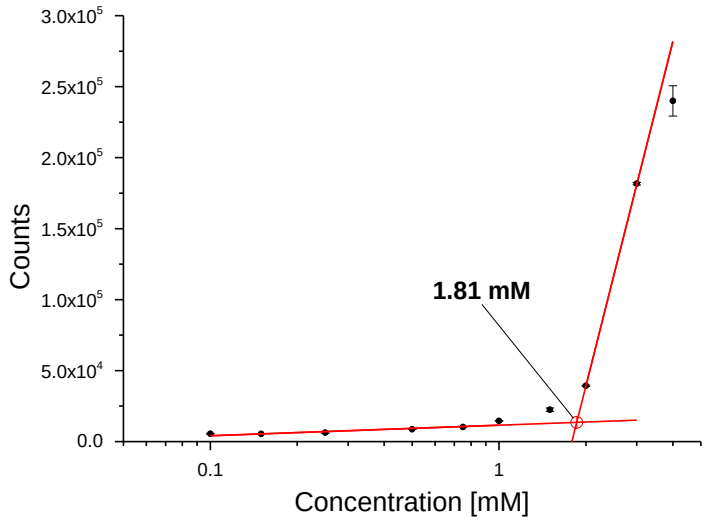

Figure S51. Counts plotted against the logarithmic concentration of APG **6**.

Table S18. CMC with nile red of APG **7**, TDS(Man)-C12.

Concentration [mM]	Ø Counts @635 nm	Standard deviation
0.1	5341	160
0.15	4906	67
0.25	5921	348
0.5	5913	89
0.75	7894	216
1	10280	200
1.5	21786	5236
2	36347	7196
3	75543	7068
4	153909	768

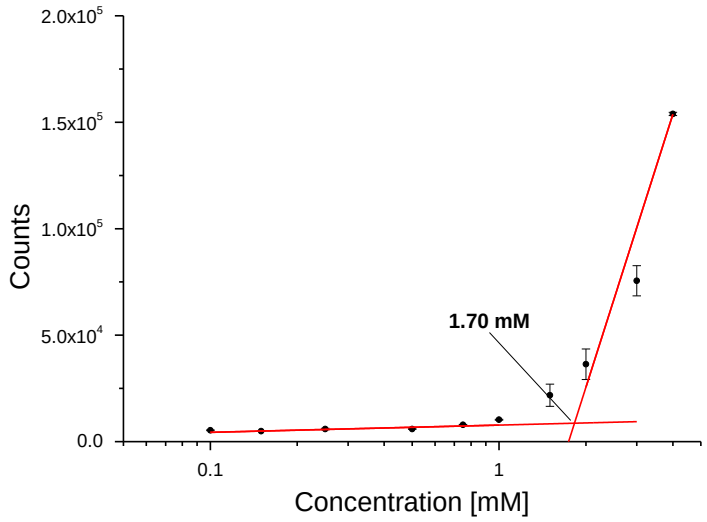

Figure S52. Counts plotted against the logarithmic concentration of APG **7**.

Table S19. CMC with nile red of APG **8**, Gly-BADS(Man)-HDM-C12.

Concentration [mM]	Ø Counts @635 nm	Standard deviation
0.1	5720	199
0.15	7760	547
0.25	12490	589
0.5	23920	503
0.75	38329	1339
1	45277	104
1.5	59144	1073
2	66831	1627
3	75281	699
4	75146	5

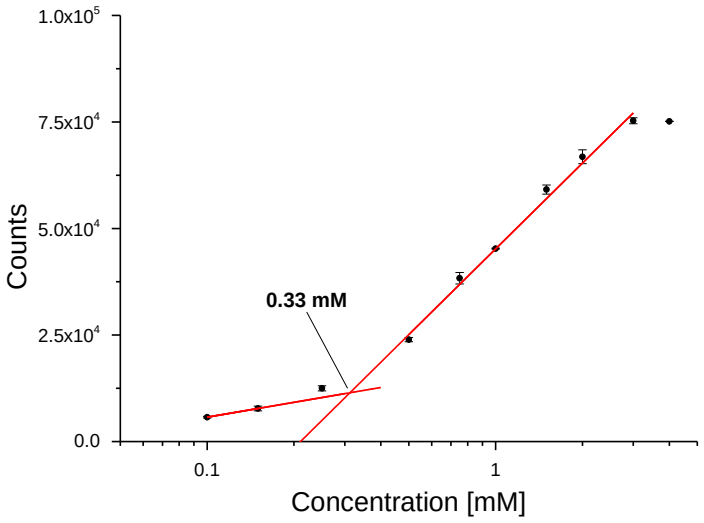

Figure S53. Counts plotted against the logarithmic concentration of APG **8**.

5. Further TEM images of APG 7

For APG 7 only small number of spherical micelles were visible using TEM. Therefore, we provide here additional images.

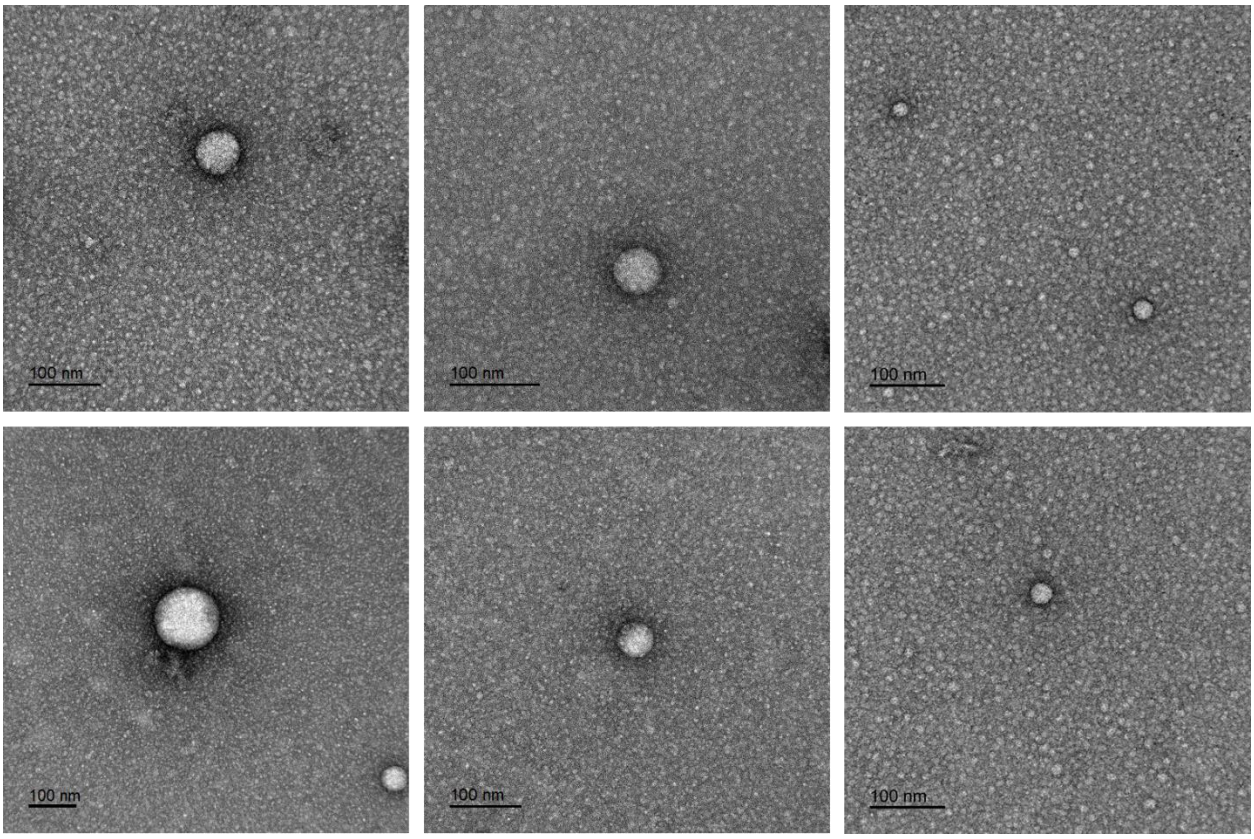

Figure S54. Additional TEM images of APG 7.

6. Crosslinking verification

To further verify the crosslinking both samples crosslinked and non-crosslinked were dispersed at the same concentration in ethanol/water 1:1 mixture and the scattered light intensity (count rate) of the DLS was measured. In this solvent mixture all non-crosslinked micelles will be dissolved and only the crosslinked micelles remain intact. In Figure S43 the

count rates and the respective correlation functions are displayed. The count rate for the crosslinked sample is about 5 times higher and the respective correlation cruve shows a typical progression. For the non-crosslinked sample, the count rate is really low and the correlation function is shifted towards smaller tau, which indicates that only unimers are present in solution.

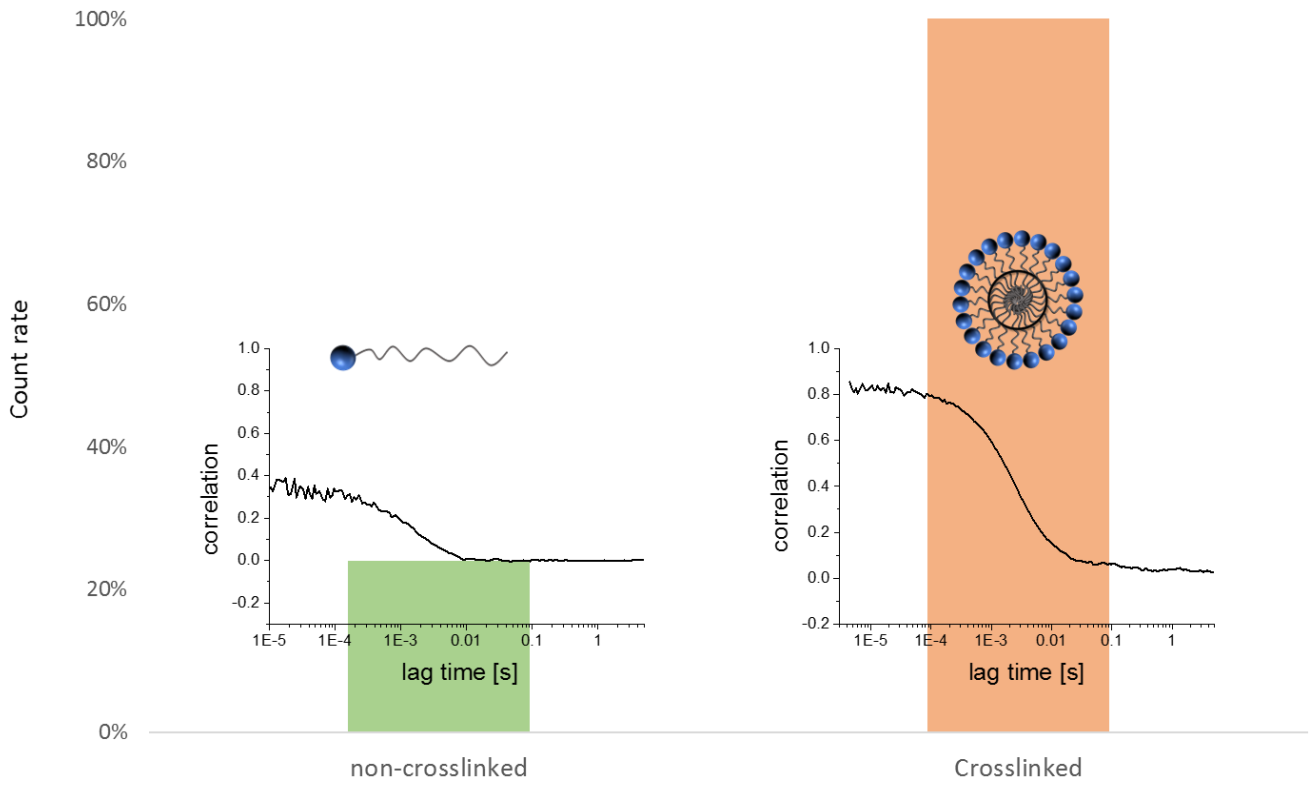

Figure S55. Comparison of the Count rate and correlation curve of non-crosslinked and crosslinked APG **8** micelles in ethanol/water mixture 1:1.

7. Fluorescence microscopy images of rhodamine label Con

A rhodamine labeled ConA stock solution of 1mg/ml was prepared in lectin binding buffer (10 mM Hepes, 50 mM NaCl, 1 mM $MnCl_2$, 1 mM $CaCl_2$, pH 7.4). 1 µL of this solution was added to a solution of 5 mM APG 8 also in LBB. This mixture was incubated for 30 minutes and afterwards directly measured with a fluorescence Microscope.

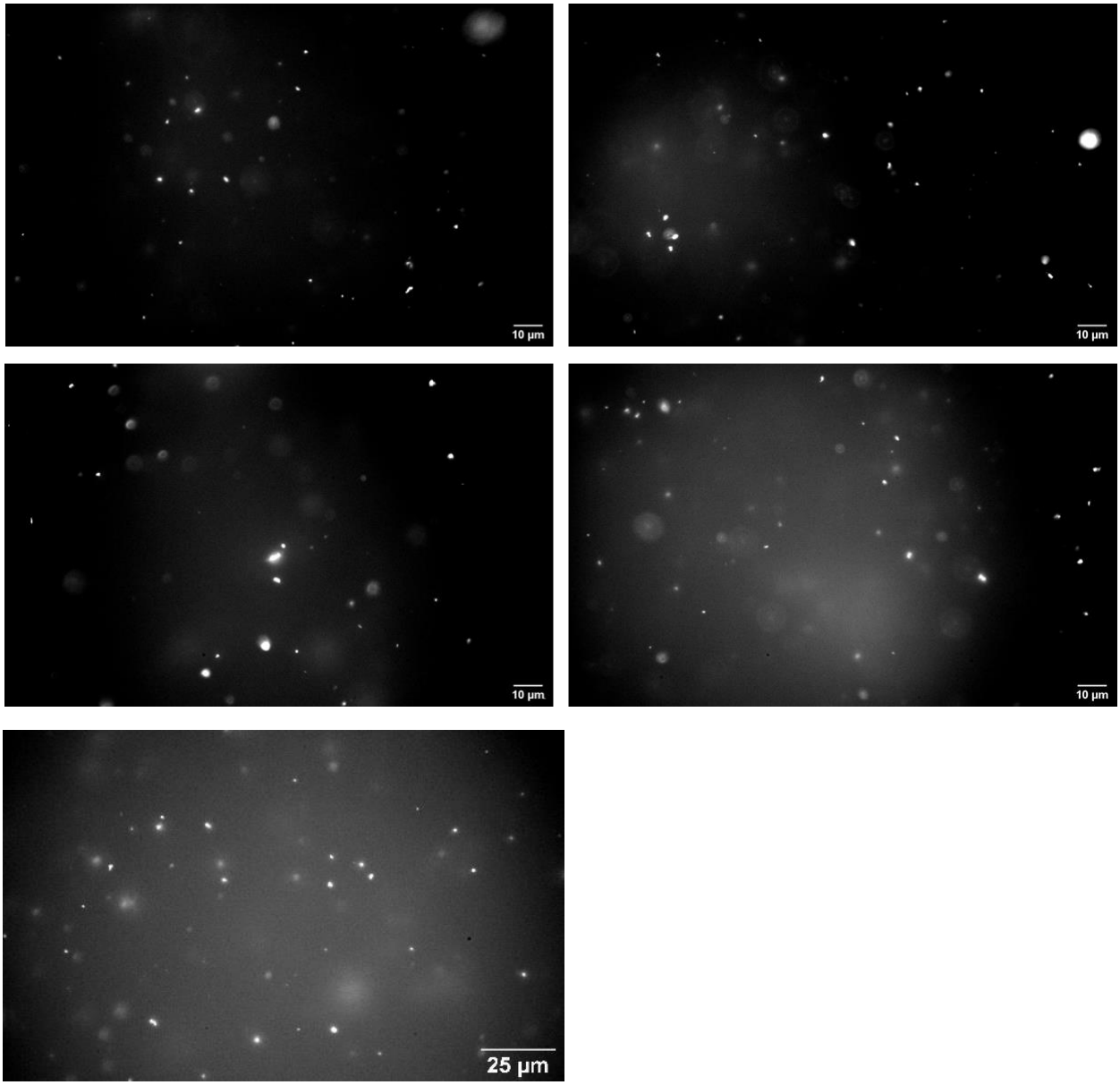

Figure S56. Fluorescence microscope image of APG **8** incubated with rhodamine conjugated ConA (post edited with ImageJ).

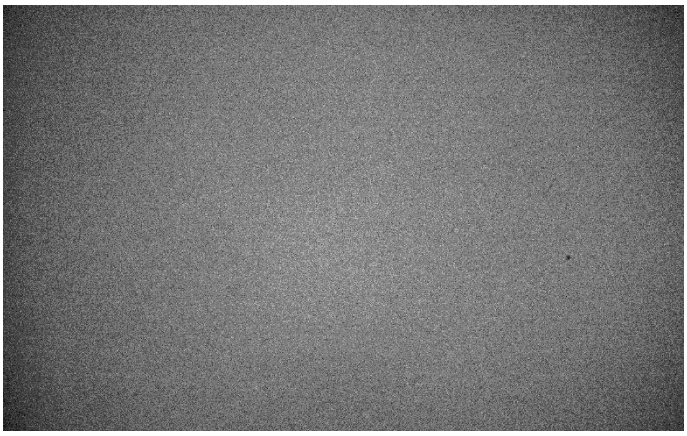

Figure S57. Picture of only APG **8** in solution under fluorescence microscope.

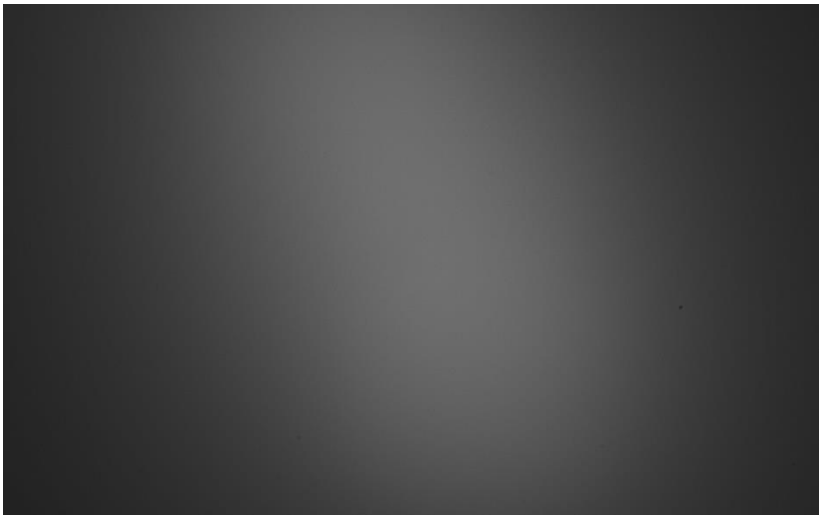

Figure S58. Fluorescence microscope image of rhodamine conjugated ConA in solution.

8. Micelle stability in PBS

8.1 CMC in PBS

APGs were dissolved in MQ water and CMCs were measured following the nile red CMC protocol. Subsequently, 10 µL of ten times concentrated PBS solution were added to each well. Wellplates were shaken and subsequently the CMC measurement was repeated.

Table S20. Overview of the CMCs in PBS

	PBS	
Structure	CMC	Deviation
APG_1	0.59	0.01
APG_3	0.06	0.004
APG_4	0.63	0.07
APG_6	0.49	0.001
APG_7	1.98	0.02
APG_8	0.3	0.01

8.2 TEM images of APGs in PBS

APG **1** and **8** were dissolved in PBS with a final concentration of 4 mM. TEM samples were prepared following the standard TEM staining protocol. Micelles were observed for APG **1** and APG **8** in PBS.

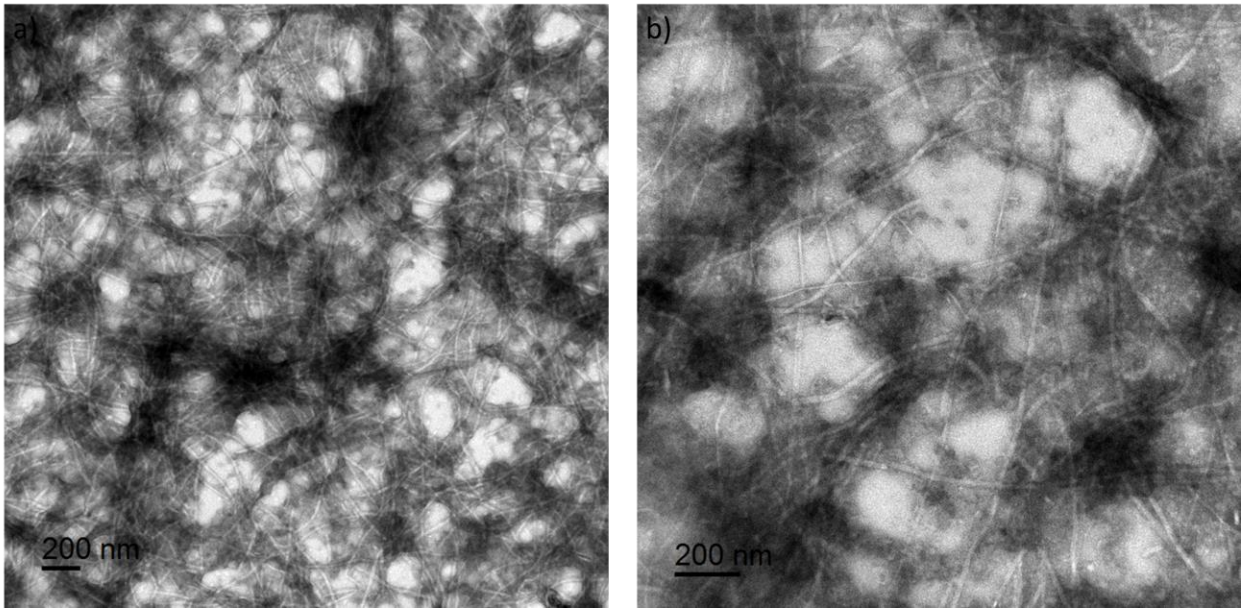

Figure S59. TEM images of a) APG **1** in PBS and b) APG **8** in PBS.

9. Bacteria adhesion assay

Experiments were conducted as described in the general methods section. All data points were averaged, corrected against the Blank (PBS) and then relative values are calculated by dividing the data against the Blank (Bacteria). APG **4** was used as negative control in all measurements.

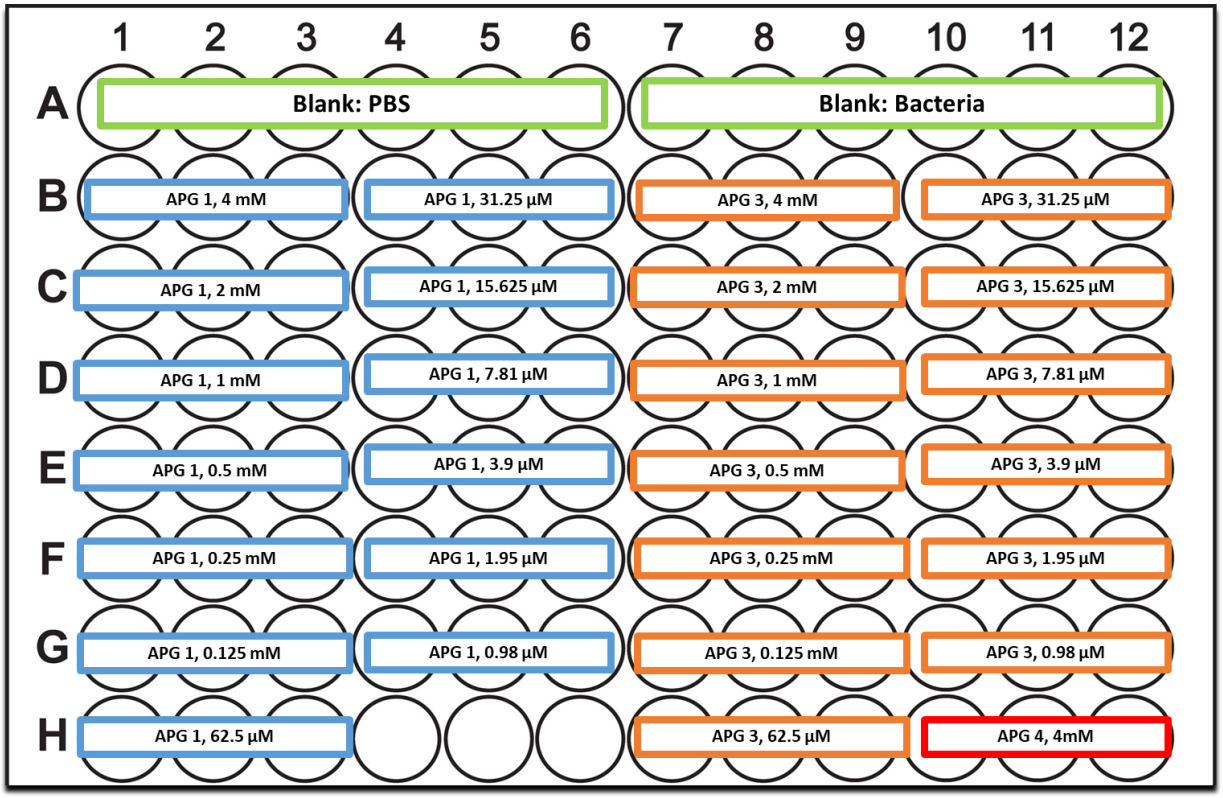

Figure S60. Standard 96-wellplate setup for the bacteria adhesion assay.

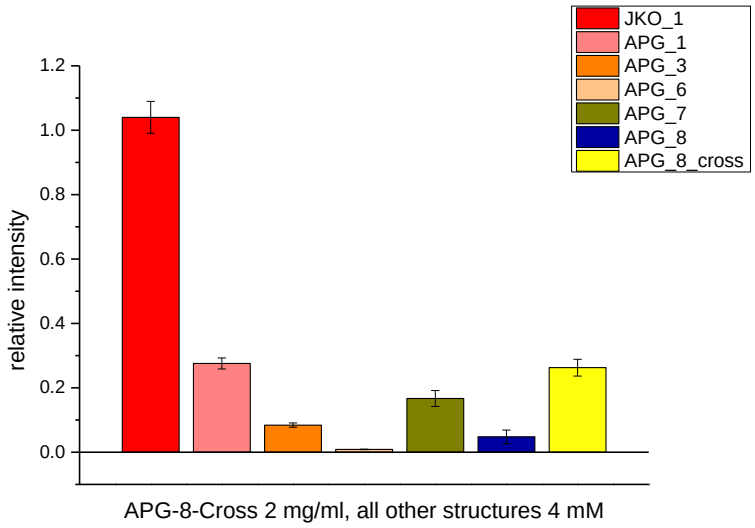

Figure S61. Inhibition of *E. coli* surface adhesion after 4.5 hour of incubation at the highest concentration of APGs.

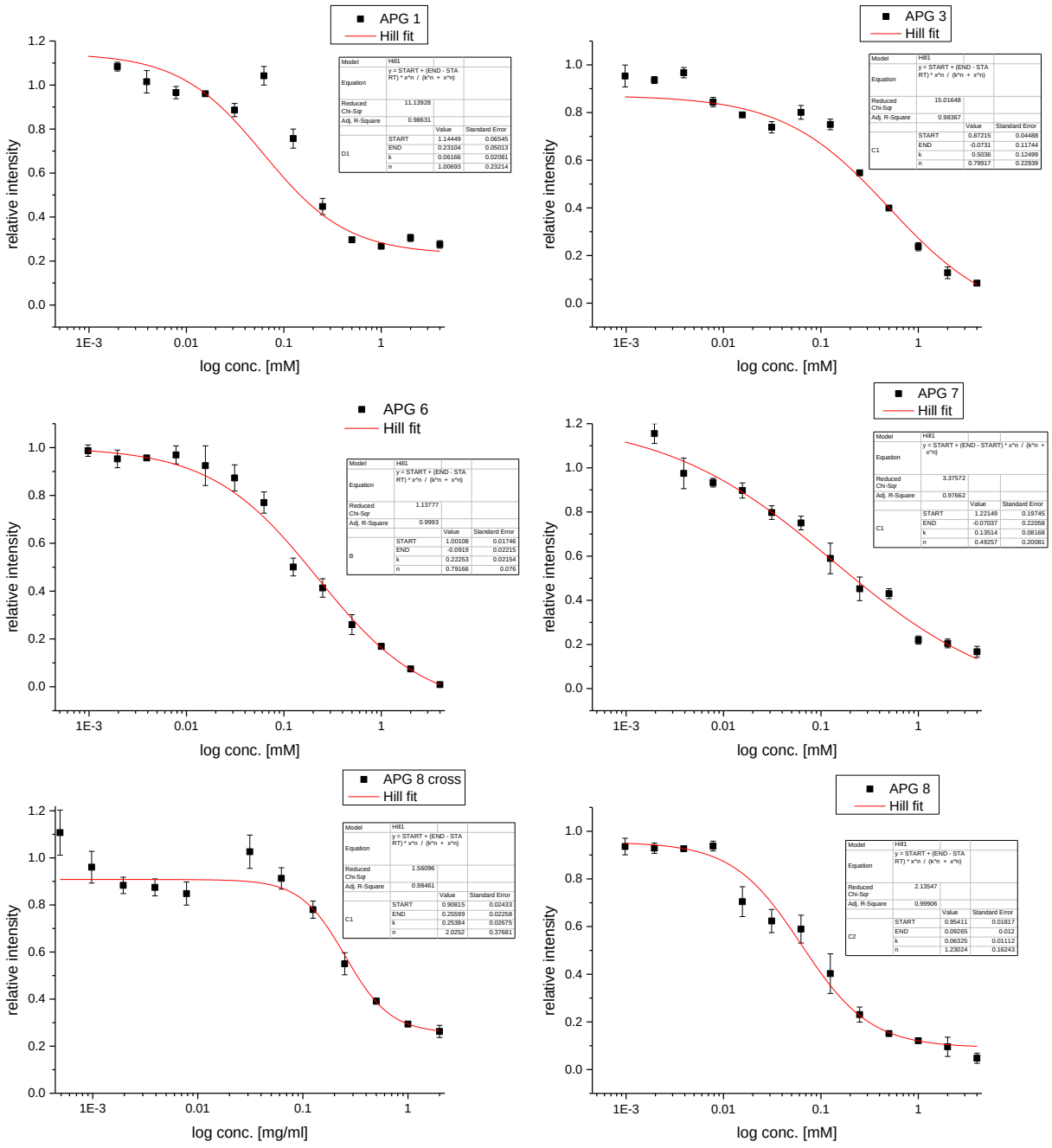

Figure S62. Inhibition curves and hill fit of APG **1**, **3**, **6, 7**, **8** and APG **8** crosslinked after 4.5 hours of incubation.

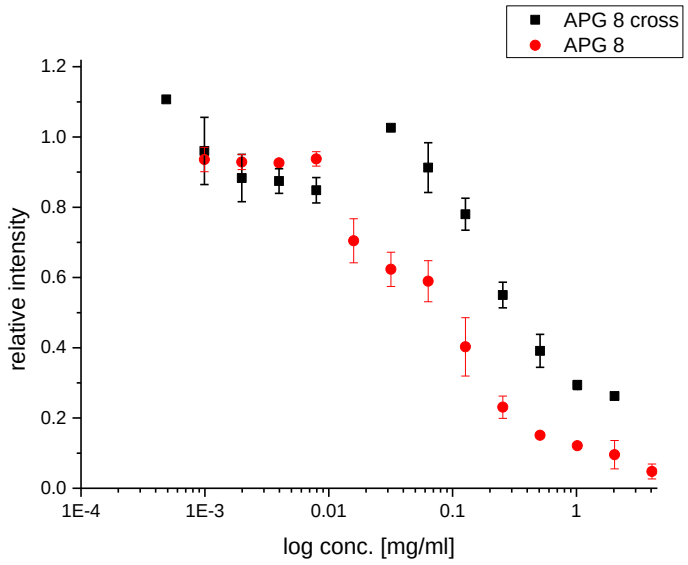

Figure S63. Comparison of the inhibitory potential in mg/ml of APG **8** crosslinked and APG **8**.

10. AFM Image of APG 5

AFM image of freshly prepared APG 5. For that APG 5 was dissolved in MQ water at 5 mM.

Subsequent 10µl were directly spin coated on prior cleaned silicon wafers.

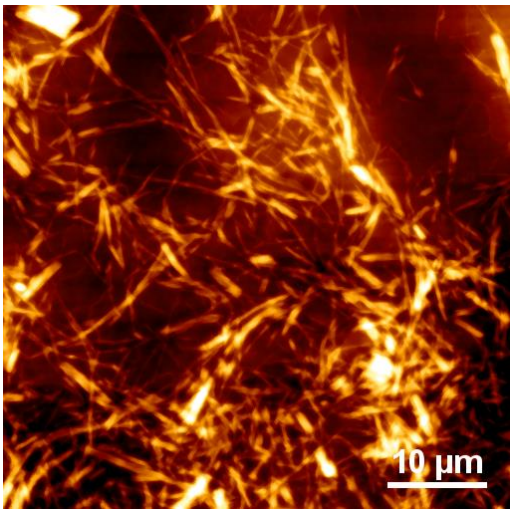

Figure S64. AFM image of a freshly prepared and spin coated sample of APG 5.

11. References

1. L. Wu and N. S. Sampson, *ACS Chem. Biol.*, 2014, **9**, 468-475.
2. D. Ponader, F. Wojcik, F. Beceren-Braun, J. Dernedde and L. Hartmann, *Biomacromolecules*, 2012, **13**, 1845-1852.
3. M. Hartmann, A. K. Horst, P. Klemm and T. K. Lindhorst, *Chem. Commun.*, 2010, **46**, 330-332.
4. B. J. Frisken, *Appl. Opt.*, 2001, **40**, 4087-4091.
5. M. Hoffmann, Y. Lu, M. Schrinner, M. Ballauff and L. Harnau, J. Phys. Chem. B, 2008, **112**, 14843-14850.
6. M. M. Tirado and J. G. de la Torre, J. Chem. Phys., 1979, **71**, 2581-2587.
7. M. M. Tirado and J. G. de la Torre, J. Chem. Phys., 1980, **73**, 1986-1993.
8. D. La Torre, J. García, M. C. L. Martinez and M. M. Tirado, *Biopolymers*, 1984, **23**, 611-615.